ChemComm

ROYAL SOCIETY OF CHEMISTRY

FEATURE ARTICLE

View Article Online
View Journal | View Issue

Check for updates

Cite this: *Chem. Commun.*, 2025, **61**, 2235

# Covalent organic frameworks for radioactive iodine capture: structure and functionality

Jie Fu, *[a] Jin-Yang Kang,[a] Wei Gao,[a] Zhi-Wen Huang,[a] Ling-Qin Kong,[a] Kai Xie,[a] Qiu-Hong Zhu,[b] Guo-Hao Zhang,[b] Guo-Hong Tao *[c] and Ling He [c]

Received 15th November 2024,
Accepted 30th December 2024

DOI: 10.1039/d4cc06092j

rsc.li/chemcomm

The adsorption of radioactive iodine is a critical concern in nuclear safety and environmental protection due to its hazardous nature and long half-life. Covalent organic frameworks (COFs) have emerged as promising materials for capturing radioactive iodine owing to their tunable porosity, high surface area, and versatile functionalization capabilities. This review provides a comprehensive overview of the application of COFs in the adsorption of radioactive iodine. We begin by discussing the sources, properties, and hazards of radioactive iodine, as well as traditional capture techniques and their limitations. We then delve into the intrinsic structures of COFs, focusing on their porosity, conjugated frameworks, and hydrogen bonding, which are pivotal for effective iodine adsorption. The review further explores various functionalization strategies, including electron-rich COFs, flexible COFs, ionic COFs, COF nanosheets, and quasi-3D COFs, highlighting how these modifications enhance the adsorption performance. Finally, we conclude with an outlook on future research directions and potential applications, underscoring the significance of continued innovation in this field. This review aims to provide valuable insights for researchers and practitioners seeking to develop advanced materials for the efficient capture of radioactive iodine.

Published on 02 mis Genver 2025. Downloaded on 06/02/2026 05:45:19.

## 1 Introduction

Since the beginning of the 21st century, the world has been facing an energy crisis brought about by population and industrial growth, as well as global warming due to greenhouse gas emissions.[1–3] In response, the number of nuclear power plants has rapidly increased worldwide, with nuclear energy

[a] *CNNC Sichuan Environmental Protection Engineering Co., Ltd., Guangyuan 628000, China. E-mail: dr.fujie@qq.com*
[b] *School of Nuclear Science and Technology, Southwest University of Science and Technology, Mianyang 621010, China*
[c] *College of Chemistry, Sichuan University, Chengdu 610064, China. E-mail: taogh@scu.edu.cn*

**Jie Fu**

*Jie Fu is an engineer of CNNC Sichuan Environmental Protection Engineering Co., Ltd. He received a Bachelor's degree in Materials Science and Engineering (2019) from China University of Geosciences (Beijing), and a PhD in Radiochemistry (2024) from Sichuan University. He became a high-level introduced engineer at CNNC Sichuan Environmental Protection Engineering Co., Ltd in July 2024. He mainly engages in research on the decommissioning of nuclear facilities and technologies for the treatment of solid radioactive waste.*

**Qiu-Hong Zhu**

*Qiu-Hong Zhu is an associate professor at the School of Nuclear Science and Technology (SWUST), Southwest University of Science and Technology. She obtained a PhD in Radiochemistry from Sichuan University in 2023. In July of the same year, she was introduced as an outstanding talent by SWUST and became a full-time researcher. Her research interests focus on intelligent switchable imine materials based on dynamic covalent chemistry, bio based porous functional materials, and their application in rapid adsorption and real-time on-site detection of radioactive elements, as well as theoretical research on dynamic covalent chemical reaction mechanisms.*

Published on 02 mis Genver 2025. Downloaded on 06/02/2026 05:45:19.

being tasked with meeting the rising energy demands and achieving carbon peak and carbon neutrality goals.[4–6] Typically, a gigawatt nuclear power plant produces approximately 25–30 tons of spent fuel annually.[7] This spent fuel is temporarily stored as radioactive waste or undergoes reprocessing. Nuclear spent fuel reprocessing is crucial for enhancing the utilization of uranium fuel and reducing the generation of high-level radioactive waste,[8] thereby playing a vital role in the sustainable development of nuclear energy. During reprocessing, spent fuel rods go through processes such as cutting, dissolving, and extraction, eventually separating into various nuclides.[9,10]

In the spent fuel dissolution solution, approximately 95% is composed of $^{238}$U, 1% is $^{235}$U, about 1–2% consists of plutonium isotopes, 2–3% are radioactive fission products (such as $^{85}$Kr, $^{129}$I, $^{3}$H, $^{137}$Cs, *etc.*), and less than 0.1% are transuranic element.[7,9] To date, most reprocessing plants worldwide use the PUREX (Plutonium and Uranium Reduction EXtraction) process for spent fuel reprocessing.[11,12] This process is employed to separate and purify uranium and plutonium from the spent fuel dissolution solution.[13] During reprocessing, a series of radioactive wastes are inevitably generated. According to the lifetimes and radiation properties of the nuclides, the International Atomic Energy Agency classifies them into five categories:[14] (1) very short-lived waste, (2) very low-level waste, (3) low-level waste, (4) intermediate-level waste, and (5) high-level waste. Different categories of radioactive nuclide waste require different disposal methods, such as short-term storage, near-surface burial, and permanent deep geological disposal after concentration.[8,15] These radioactive nuclides not only directly damage the ecological environment but can also be transmitted to humans through the food chain,[16,17] affecting metabolic processes and causing a range of severe diseases. Consequently, once released into the environment, they can become a global disaster.

Among them, volatile radioactive iodine ($^{129}$I and $^{131}$I) poses a higher potential threat to the environment and ecology due to their strong migration and diffusion capabilities and the difficulty in controlling them.[18–20] Therefore, they must be safely and effectively separated, immobilized, and permanently isolated. Covalent organic frameworks (COFs) offer promising characteristics for this purpose due to their tunable porosity, high surface area, chemical stability, and ease of functionalization.[21–23] These properties enable COFs to effectively capture and immobilize radioactive iodine molecules,[24,25] reducing their mobility and potential impact on human health and the environment. Additionally, the modular nature of COFs allows for the design of tailored materials with enhanced adsorption capacities and selectivity,[26,27] making them promising candidates for addressing the challenges associated with radioactive iodine adsorption.

## 2 Covalent organic frameworks

Covalent organic frameworks (COFs) are a class of crystalline materials characterized by their ordered porous structures.[28–32]

**Guo-Hao Zhang**

*Guo-Hao Zhang is an associate professor at the School of Nuclear Science and Technology, Southwest University of Science and Technology. He obtained a Bachelor's degree in Chemistry from Sichuan University in 2018 and a PhD in Radiochemistry from Sichuan University in 2023. He became a high-level introduced researcher at Southwest University of Science and Technology in July 2023. He is mainly dedicated to the design and synthesis of polymer materials functionalized with ionic liquids, as well as their application research in gaseous environmental pollutants including radioactive iodine, fine particulate matter, aerosols, etc.*

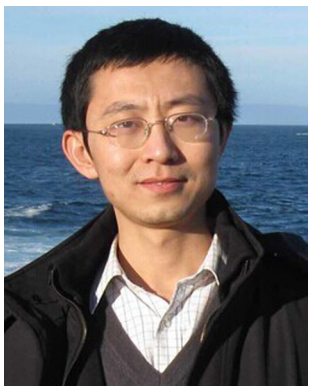

**Guo-Hong Tao**

*Guo-Hong Tao is a Professor of Chemistry at Sichuan University. He received a Bachelor's degree in Chemistry (2001) from Lanzhou University, and a PhD in Physical Chemistry (2006) from Peking University. He completed postdoctoral research in the team of Prof. Jean'ne M. Shreeve at the University of Idaho and became a principal investigator in Sichuan University in 2010. He is mainly devoted to the fundamental and applied research of ionic liquids, especially their applications in high-tech and high value-added fields such as energy materials, safe/eco-friendly materials, and smart materials.*

**Ling He**

*Ling He is a Professor of Chemistry at Sichuan University. She received a Bachelor's degree in Chemistry (2003) at Sichuan University, and a PhD (2008) in Physical Chemistry at Peking University. She was a postdoctoral fellow at the University of Idaho (2008–2010) and a Visiting Scholar at the University of Colorado, Boulder (2018–2019). She started her independent career as an associate professor at Sichuan University in 2010. Her main research interests are the genome of ionic functional materials, the construction of ionic network materials, and their applications in the fields of radiochemistry, environment, and energy.*

 This journal is © The Royal Society of Chemistry 2025

Published on 02 mis Genver 2025. Downloaded on 06/02/2026 05:45:19.

They are formed by the polymerization of light elements (such as C, H, N, O, S, and P) through thermodynamically controlled reversible covalent bonds.[33–36] Compared to traditional organic polymer materials, COFs exhibit several advantageous properties, including low density, excellent chemical stability, high specific surface area, well-defined porous structures, and ease of functionalization.[22,23,37–39] Leveraging these advantages, COFs have recently gained prominence in the fields of gas adsorption, storage, and conversion.[21,28,40–44]

COFs are constructed from rigid building block monomers with symmetrical reactive groups at their vertices or edges, connected through condensation reactions.[45] They are denoted as $C_n$ based on the number of symmetrical reactive groups (n). These building block monomers typically have specific topological structures, and different combinations of these monomers result in various polygonal framework structures (Fig. 1).[46,47] For example, the combination of a $C_3$ symmetric vertex (1,3,5-triformylphloroglucinol) and a $C_2$ symmetric vertex (1,4-phenylenediamine) forms a COF with a hexagonal pore structure, such as TpPa.

COFs can be categorized into two-dimensional (2D) COFs and three-dimensional (3D) COFs, each with unique porous structures derived from their topological frameworks.[48] In 2D COFs, building units are periodically connected by covalent bonds and stacked through π–π interactions, forming crystalline layered structures.[49] These stacked structures feature one-dimensional (1D) channels with sizes and shapes that can be tuned by altering the building units.[50] To form highly ordered frameworks, the covalent bonds in COFs should exhibit a certain degree of reversibility during synthesis to ensure self-correction. Various types of linkage bonds are used in COFs, with boronate ester, imine, nitrone and olefinic linkages being the most common. These linkages directly affect the stability and intrinsic properties of COFs.[37]

Boronate ester-linked COFs, for instance, often exhibit luminescence due to the electron-deficient nature of boron, but this also leads to instability in high humidity.[51] Imine-linked COFs, on the other hand, demonstrate greater stability compared to boronate ester-linked COFs.[52,53] In iodine adsorption studies, iodine molecules, as typical electrophilic species, can be effectively adsorbed by the lone pair electrons on nitrogen atoms in imine linkages.[54,55] These electrons can transfer to the antibonding orbital (σ*) of iodine, forming charge-transfer complexes.[56,57] For enhanced stability, Yaghi and colleagues[29] synthesized COFs based on olefinic double bonds, which showed significantly improved stability and crystallinity under both strongly acidic and basic conditions. However, the synthesis of these COFs is challenging and requires stringent conditions.[58] In contrast, imine-linked COFs offer a balanced combination of ease of synthesis, good stability, and inherent electron-rich sites, making them a focal point in research on the adsorption of radioactive iodine.[24,59]

To date, over 100 imine-linked COF-based iodine adsorbents have been reported.[33,60,61] Typical examples of symmetrical monomers with aldehyde and amino functional groups used for synthesizing imine bonded COFs are shown in Fig. 2. These COFs possess unique intrinsic porous structures, and their physical and chemical properties can be tuned through appropriate functionalization. Various functionalization methods effectively introduce active sites for iodine adsorption, enhancing their capacity to capture iodine. In 2017, Zhao *et al.*[62] reported the first COF adsorbent for iodine adsorption. They introduced a novel hollow microspherical COF with heteroporous 2D structures (SIOC-COF-7). Thanks to the large internal cavity and inherent heteroporous structure of the COF microspheres, SIOC-COF-7 achieved a saturated iodine adsorption capacity ($Q_e$) of 4.81 g $g^{-1}$. The study indicated that the

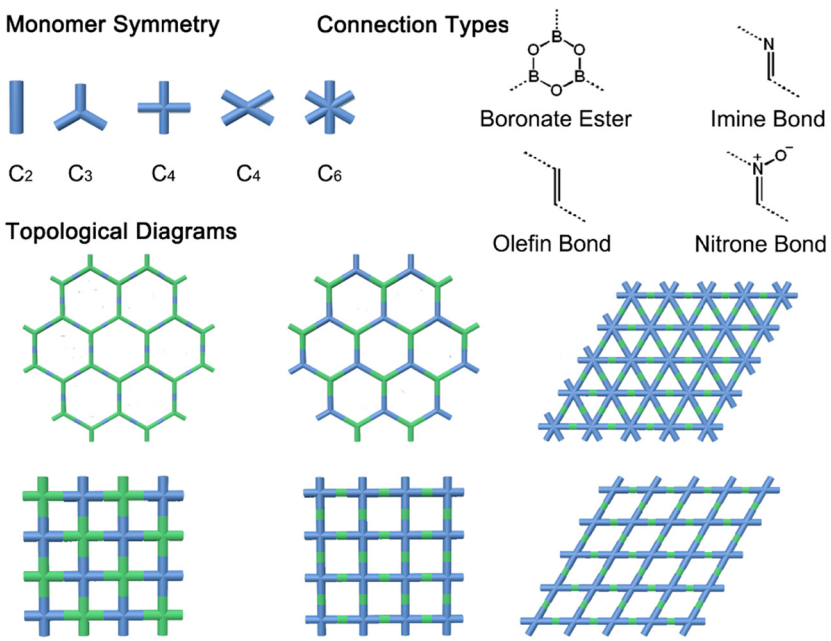


Fig. 1 Basic topological diagrams and connection types of some representative two-dimensional COFs.

Published on 02 mis Genver 2025. Downloaded on 06/02/2026 05:45:19.

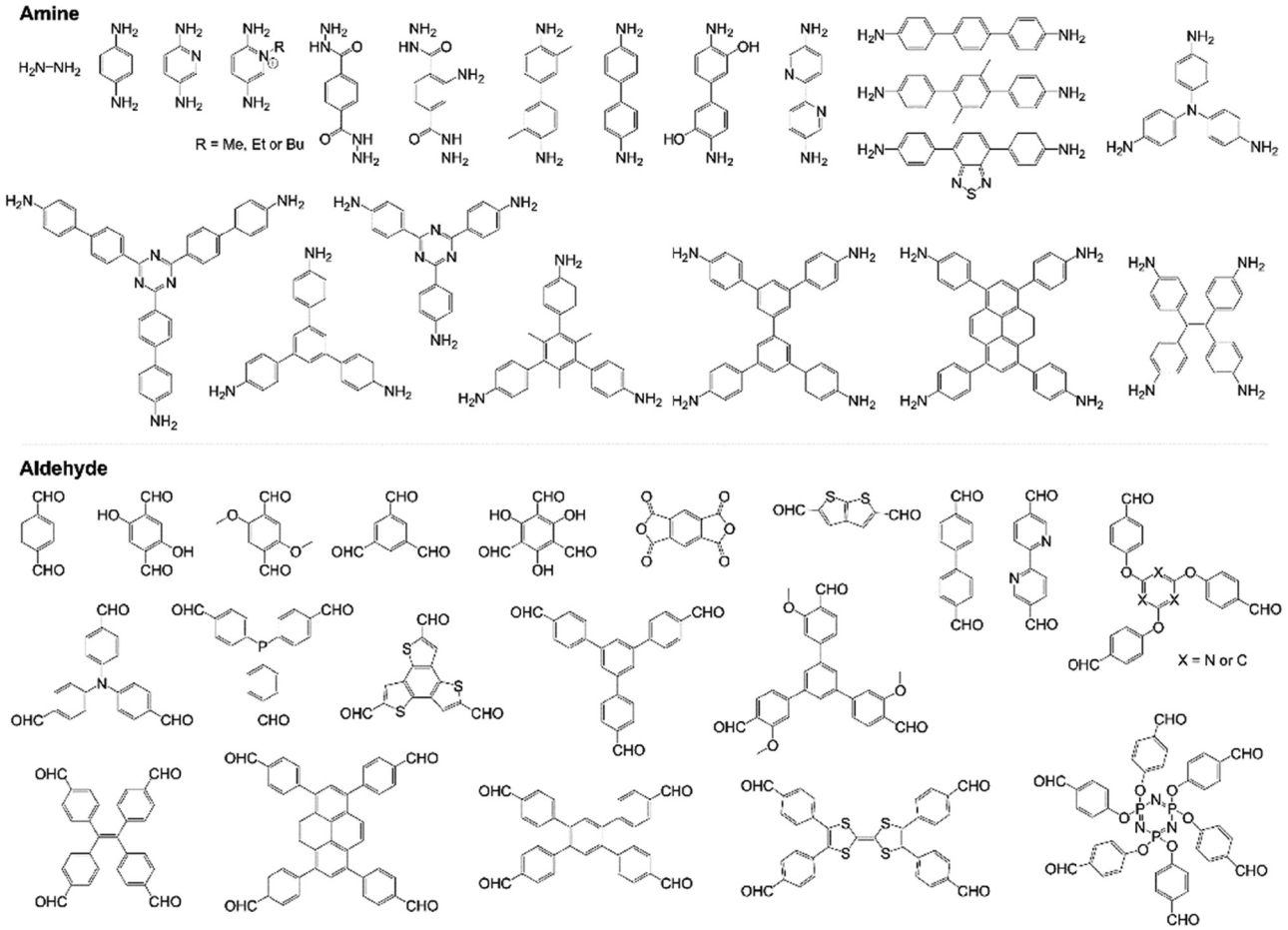


Fig. 2 Typical examples of symmetrical monomers with aldehyde and amino functional groups used for synthesizing imine bonded COFs.

abundant aromatic rings, nitrogen heteroatoms, and orderly framework network in the heteroporous SIOC-COF-7 facilitated iodine adsorption. Additionally, the highly ordered pore structure within the hollow microspheres' cavity and shell layer significantly contributed to effective iodine capture. Following this breakthrough, numerous successful cases of COFs for gaseous iodine capture were reported. In 2018, Jiang *et al.*[24] published an article in Advanced Materials highlighting the unexpectedly high iodine adsorption capacity of 2D COFs, drawing attention from material scientists and radiochemists worldwide, and marking the initial development phase of COF-based iodine adsorption. In 2020, Wang and Han *et al.*[63] proposed nitrogen-rich functionalized COFs for dynamic iodine adsorption. That same year, Ma *et al.*[64] introduced the use of the $k_{80\%}$ value to describe the average adsorption rate of COF adsorbents, which gained widespread recognition and application in the academic community. In 2021, Ma *et al.*[65] proposed flexible COF adsorbents that adaptively regulate according to the size of guest molecules, defining the concept of flexibility in host–guest interactions. Han *et al.*[66] reported the first ionic COF-based iodine adsorbent in the same year, achieving a breakthrough in $Q_e$ by reaching 10.21 g $g^{-1}$, surpassing the 10 g $g^{-1}$ mark for the first time. The current highest adsorption capacity is 10.81 g $g^{-1}$, maintained by ECUT-COF-13, as reported by Luo *et al.*[67] In 2023, Tao and He *et al.*[68] reported the first study on iodine adsorption using ionic COF nanosheets, making significant progress in adsorption rates. Zhang *et al.*[69] reported the synthesis of two novel nitrones-linked COFs (CityU-1 and CityU-2) through the Kröhnke oxidation reaction. Fig. 3 shows the timeline of key COF studies related to radioactive iodine adsorption. Although research on COFs for iodine capture is still in its early stages, COFs exhibit exceptional core competitiveness in iodine capture due to their unique structural features, such as tunable pore sizes, high specific surface areas, and high crystallinity. The potential for future applications is immense.

COFs utilize nitrogen atoms, oxygen atoms, and other heteroatoms as the primary sites for iodine adsorption.[34,70] These heteroatoms can form charge-transfer complexes with iodine molecules, enhancing the adsorption capability.[56,57,71] For instance, in COFs connected by imine bonds, the Lewis acid–base interaction between polar C–N bonds and iodine molecules improves the material's iodine capture ability.[24] The well-ordered and regular pore structure of COFs facilitates the thorough penetration and adsorption of iodine molecules within the material.[72] Compared to other porous materials,

 This journal is © The Royal Society of Chemistry 2025

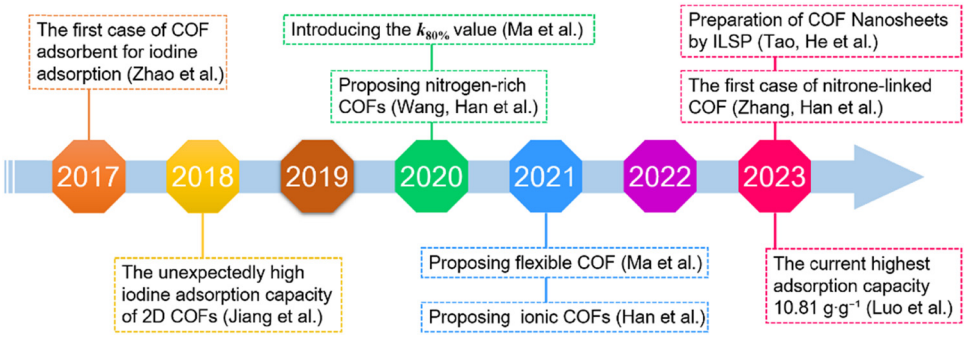


Fig. 3 A schematic diagram showing the timeline of key COF studies related to radioactive iodine adsorption.

Published on 02 mis Genver 2025. Downloaded on 06/02/2026 05:45:19.

the pores in COFs are less susceptible to clogging, enabling them to maintain high adsorption efficiency.

The iodine adsorption process in COFs encompasses both physical and chemical adsorption mechanisms. Physical adsorption is primarily driven by van der Waals forces between iodine molecules and the pore walls of COFs.[24,72] Chemical adsorption involves the formation of charge-transfer complexes or ionic iodides (*e.g.*, $I_3^-$ and $I_5^-$) through interactions between iodine molecules and heteroatoms in the COFs.[25,73,74] COFs generally exhibit a rapid iodine adsorption rate, often reaching equilibrium within a short time. This adsorption rate is influenced by factors such as the pore structure, heteroatom content, and iodine molecule concentration in the COFs.

The size, shape, and distribution of pores in COFs significantly influence the entry and adsorption efficiency of iodine molecules. Similarly, the type and content of heteroatoms play a critical role in determining the iodine adsorption performance of COFs. Environmental factors, such as temperature, pressure, and humidity, also impact the adsorption capabilities. To address these challenges, researchers have proposed various optimization strategies. By tailoring the building blocks and synthesis conditions of COFs, it is possible to fine-tune their pore structures and heteroatom content, thereby enhancing their iodine adsorption efficiency. Post-synthesis modifications or functionalization of COFs can introduce additional adsorption sites or strengthen interactions with iodine molecules. A Summary of the adsorption performance of various COFs for radioactive iodine is shown in Table 1. This review paper provides a comprehensive analysis of these approaches in Sections 4 and 5.

# 3 Radioactive iodine

Understanding the generation, properties, hazards, and species distribution of radioactive iodine is crucial for guiding the design, synthesis, and practical application of COF-based iodine adsorbents. Nuclear fission reactions in reactors produce fission and activation products, some of which are volatile under spent fuel reprocessing conditions.[91] Identified as "volatile radioactive nuclides" are rare gases (mainly isotopes of Kr and Xe), $^3$H, $^{14}$C, and $^{129}$I.[92,93] During wet reprocessing processes, these radioactive nuclides mostly enter the off-gas stream as tritiated water ($^3$HHO or $^3H_2O$), radioactive $^{14}CO_2$, rare gases (mainly $^{85}$Kr), and gaseous iodine ($^{129}I_2$, H$^{129}$I, or organic iodides).[94,95] The United States was among the first countries to research and implement nuclear fuel cycles. Over the past 50 years, various materials have been developed and tested for capturing and immobilizing volatile radioactive nuclides. Despite these efforts, no material has yet achieved the most satisfactory performance and economic viability.[94] Their research indicates that controlling the release of $^{129}$I is critical due to its long half-life of $1.57 \times 10^7$ years and significant potential biological threat. Therefore, $^{129}$I emission control is essential in managing volatile radioactive nuclides.

## 3.1 Sources of radioactive iodine

Human nuclear tests are one source of radioactive iodine. Studies have found that each kiloton of TNT equivalent of $^{235}$U or $^{239}$Pu fission during an explosion produces approximately 0.17 grams and 0.28 grams of $^{129}$I, respectively.[96] However, most radioactive iodine is generated in nuclear power reactors. $^{129}$I is one of the longest-lived radioactive nuclides produced in the nuclear fuel cycle.[97] It is a fission product of $^{235}$U and $^{239}$Pu in reactors and continuously accumulates in them. It is estimated that a nuclear power reactor generates about 7.3 milligrams of $^{129}$I per megawatt-day of energy produced.[98] Due to its unique physical, chemical, and biological properties, without preventive measures, $^{129}$I would eventually be released into the natural environment through the emissions of off-gas from spent fuel reprocessing plants. This would result in its distribution across various environmental media such as the atmosphere, water bodies, soil, and the food chain.[19] Given the extremely long half-life of $^{129}$I, no engineering barrier can permanently isolate it. Consequently, since the inception of spent fuel reprocessing research, the optimal capture technologies and final management strategies for $^{129}$I have been focal points in the fields of reprocessing and environmental radiochemistry, and this remains an evolving frontier.

$^{131}$I, produced in fast reactors, is a spontaneous fission product of $^{244}$Cm and does not occur naturally.[99] With a half-life of only 8 days, conventional methods to control $^{131}$I release involve increasing the cooling time of spent fuel and delaying reprocessing (usually for 180–220 days).[100] However, special

Published on 02 mis Genver 2025. Downloaded on 06/02/2026 05:45:19.

Table 1 Summary of the adsorption performance of various COFs for radioactive iodine

| No. | COFs | $Q_e$ (g g$^{-1}$) | $k_{80\%}$ (g g$^{-1}$ h$^{-1}$) | Ref. |
|---|---|---|---|---|
| 1 | Th-Bta COF | 0.68 | — | 70 |
| 2 | TpPaSO$_3$H | 1.5 | 0.51 | 68 |
| 3 | USTB-4 | 1.5 | — | 34 |
| 4 | COF-TpgTd | 1.66 | — | 75 |
| 5 | COF-TpgBD | 1.81 | — | 75 |
| 6 | Hz-COF(C═N) | 2.05 | — | 76 |
| 7 | TPT-Azine-COF | 2.19 | — | 77 |
| 8 | TP-PDA-COF | 2.2 | — | 26 |
| 9 | TPT-TAPB-COF | 2.25 | — | 77 |
| 10 | TpPa-1 | 2.45 | — | 78 |
| 11 | NH-COF(C–N) | 2.6 | — | 76 |
| 12 | COF-TpgDB | 2.75 | — | 75 |
| 13 | BTT-TAPT-COF | 2.76 | — | 74 |
| 14 | QTD-COF-2 | 2.87 | 0.46 | 64 |
| 15 | Micro-COF-1 | 2.9 | — | 72 |
| 16 | COF-Ph | 3 | — | 27 |
| 17 | USTB-4c | 3.02 | — | 34 |
| 18 | C-TP-PDA-COF | 3.05 | — | 26 |
| 19 | USTB-3 | 3.14 | — | 34 |
| 20 | USTB-3c | 3.3 | — | 34 |
| 21 | Meso-COF-4 | 3.3 | — | 72 |
| 22 | DpTd-COF | 3.43 | — | 79 |
| 23 | Micro-COF-2 | 3.5 | — | 72 |
| 24 | RIL-COF-4(C═N) | 3.57 | — | 65 |
| 25 | NH2-Th-Bta COF | 3.58 | — | 70 |
| 26 | RIL-COF-2(C═N) | 3.72 | — | 65 |
| 27 | TPT-DHBD COF | 3.88 | — | 80 |
| 28 | Meso-COF-3 | 4 | — | 72 |
| 29 | TFPB-BPTA-COF | 4.02 | — | 81 |
| 30 | TAPD-DHTA COF | 4.02 | — | 82 |
| 31 | ECUT-COF-10 | 4.23 | 0.28 | 67 |
| 32 | TP-BPDA-COF | 4.3 | — | 26 |
| 33 | FAL-COF-4(C–N) | 4.36 | — | 65 |
| 34 | USTB-2 | 4.38 | — | 34 |
| 35 | TTF-TD-COF | 4.38 | — | 83 |
| 36 | FAL-COF-2(C–N) | 4.41 | — | 65 |
| 37 | USTB-1 | 4.45 | 0.22 | 34 |
| 38 | COF-PA | 4.47 | 1.3 | 27 |
| 39 | DaTd-COF | 4.48 | — | 79 |
| 40 | AC4trimTpPaSO$_3$ | 4.5 | 2.1 | 68 |
| 41 | USTB-2c | 4.57 | — | 34 |
| 42 | RIL-COF-3(C═N) | 4.62 | — | 65 |
| 43 | QTD-COF-1 | 4.62 | 1.23 | 64 |
| 44 | COF-DL229 | 4.7 | — | 84 |
| 45 | SIOC-COF-7 | 4.81 | 0.26 | 62 |
| 46 | TJNU-202 | 4.82 | — | 85 |
| 47 | QTD-COF-4 | 4.85 | 1.29 | 64 |
| 48 | DbTd-COF | 4.93 | — | 79 |
| 49 | RIL-COF-1(C═N) | 4.94 | — | 65 |
| 50 | TTA-TTB COF | 4.95 | — | 24 |
| 51 | TFB-Td | 4.97 | — | 86 |
| 52 | TTF-TAPT-COF | 5.02 | — | 83 |
| 53 | TAPD-PDA COF | 5.09 | — | 82 |
| 54 | TAPA-PDA COF | 5.09 | 1.08 | 87 |
| 55 | PA-TT-COF | 5.1 | — | 88 |
| 56 | QTD-COF-3 | 5.16 | 0.91 | 64 |
| 57 | JUC-560 | 5.2 | — | 89 |
| 58 | Bmim-TpPaSO$_3$ | 5.25 | 2.86 | 90 |
| 59 | COF-LZU1 | 5.3 | — | 78 |
| 60 | TJNU-204 | 5.33 | — | 59 |
| 61 | TPT-BD COF | 5.43 | — | 80 |
| 62 | FAL-COF-3(C–N) | 5.46 | — | 65 |
| 63 | FAL-COF-1(C–N) | 5.49 | — | 65 |
| 64 | TAPD-DMTA COF | 5.54 | — | 82 |
| 65 | ECUT-COF-11 | 5.62 | 0.45 | 67 |
| 66 | TFPB-PyTTACOF | 5.62 | — | 81 |
| 67 | TJNU-201 | 5.625 | 0.225 | 85 |
| 68 | iCOF-AB-100 | 5.76 | 1.56 | 66 |
| 69 | USTB-1c | 5.8 | 0.28 | 34 |
| 70 | COF-OH-100 | 5.85 | 0.149 | 66 |
| 71 | TJNU-203 | 5.885 | — | 59 |
| 72 | PB-TT-COF | 5.97 | — | 88 |
| 73 | SCU-COF-2 | 6 | 0.25 | 63 |
| 74 | C-TP-BPDA-COF | 6.11 | — | 26 |
| 75 | P-COF | 6.19 | — | 73 |
| 76 | TFB-BD | 6.23 | — | 86 |
| 77 | TPB-DMTP COF | 6.29 | 0.17 | 24 |
| 78 | QTD-COF-V | 6.29 | 2.51 | 64 |
| 79 | COF-OH-0 | 6.31 | 0.179 | 66 |
| 80 | TFB-DB | 6.4 | — | 86 |
| 81 | COF-OH-50 | 6.49 | 0.189 | 66 |
| 82 | ECUT-COF-12 | 7.85 | 0.6 | 67 |
| 83 | COF-TAPB | 7.94 | 0.33 | 25 |
| 84 | JUC-561 | 8.19 | — | 89 |
| 85 | COF-TAPT | 8.61 | 0.48 | 25 |
| 86 | iCOF-AB-50 | 10.21 | 1.195 | 66 |
| 87 | ECUT-COF-13 | 10.81 | 1.4 | 67 |

circumstances such as the extraction of specific fission products or transuranic elements (fast reactor reprocessing), or cladding failures, necessitate the reprocessing of short-cooled nuclear fuel. The development of materials or technologies for the isolation of $^{131}$I is also a focus area, especially in radiation medicine and radiopharmaceuticals.[101]

### 3.2 The properties and hazards of radioactive iodine

During the processes of cutting, dissolving, and extracting spent fuel, various volatile and semi-volatile radioactive nuclides are produced. These volatile radioactive iodine isotopes typically mix into the off-gas of the dissolution solution. Their unique distribution and chemical properties make them difficult to remove.[102] $^{129}$I is a long-lived nuclide with a half-life of $1.57 \times 10^7$ years and a specific activity of 0.16 mCi g$^{-1}$. It undergoes spontaneous β-decay, producing stable $^{129}$Xe as a daughter nuclide.[103] While $^{131}$I is a short-lived nuclide with a half-life of 8.02 days and a specific activity of $1.2 \times 10^8$ mCi g$^{-1}$. It also decays *via* β-decay, with stable $^{131}$Xe as the daughter nuclide.[104]

Radioactive iodine is highly volatile; during spent fuel reprocessing, it escapes from spent fuel or dissolution solutions in gaseous forms, including $I_2$, HI, and organic iodides (*e.g.*, $CH_3I$).[105] In the off-gas of the dissolution solution, over 95% of the radioactive $^{129}$I exists as $^{129}I_2$.[106] Iodine is a sensitive redox agent and participates in the formation of numerous organic and inorganic compounds in nature. It is also a bioactive element involved in synthesizing various biological organic substances such as proteins and polyphenols.[96] The human body contains numerous organs and tissues capable of absorbing iodine, with thyroid cells being the most efficient at concentrating iodine. Once radioactive iodine is inhaled or ingested, it deposits and accumulates in the thyroid, potentially leading to thyroid disorders due to prolonged internal radiation exposure.[107] Studies indicate that individuals living near early reprocessing plants (without radioactive off-gas control systems) in the United States had a higher relative risk of developing thyroid cancer.[108,109]

 This journal is © The Royal Society of Chemistry 2025

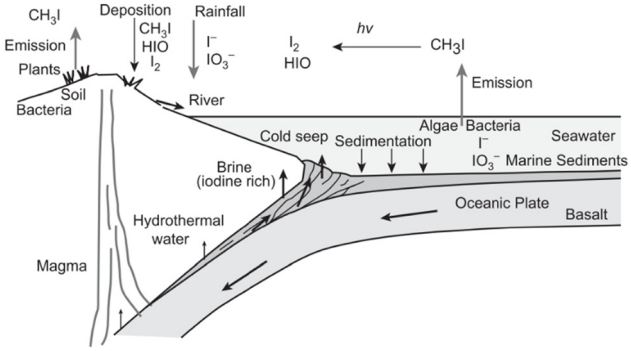


Fig. 4 The global iodine cycle. Reproduced with permission from ref. 18. Copyright©2014 Elsevier Inc.

Published on 02 mis Genver 2025. Downloaded on 06/02/2026 05:45:19.

Besides, Radioactive iodine also possesses strong migration and diffusion capabilities. Once released into the air, it cycles through water bodies, soil, air, and living organisms (as shown in Fig. 4). Radioactive iodine can be emitted into the atmosphere as molecular iodine, inorganic iodides, or organic iodides. During this process, molecular iodine can adsorb onto submicron particles.[110] All forms of radioactive iodine diffuse in the atmosphere through natural processes such as turbulence, thermal convection, and wind.[18,20,111] They eventually settle on the surfaces of plants, soil, and water bodies due to environmental factors such as rainfall. Given the extremely long half-life of $^{129}I$, its potential radiation threat is intolerable for both natural ecosystems and human health. Therefore, all possible measures must be taken to prevent the release of radioactive iodine in off-gas into the air.

### 3.3 Species distribution of radioactive iodine

Fully understanding the causes and distribution of radioactive iodine in the reprocessing process is crucial for designing and constructing highly efficient and precise capture materials or devices for radioactive iodine. The PUREX process is the predominant wet reprocessing method for spent nuclear fuel worldwide, primarily used for the separation and purification of uranium and plutonium from spent fuel.[9,13] In this process, the spent fuel undergoes cutting, and then the spent fuel fragments are dissolved in boiling concentrated nitric acid in a dissolution tank.

Studies conducted in both real and simulated experimental environments have shown that in the highly oxidizing concentrated nitric acid environment, when all fission products and actinides are completely dissolved, radioactive iodine almost entirely volatilizes from the solution and is released into the off-gas of the dissolution solution in the form of molecular iodine (accounting for 95–99% of the total iodine).[99] About 2–3% of radioactive iodine remains dissolved in the solution as iodide.[112] For instance, in the Karlsruhe reprocessing plant in Germany, the concentration of soluble iodine in spent fuel dissolution solution ranges from 1–4 mg $L^{-1}$.[106] During subsequent reprocessing steps, particularly in the TBP (tributyl phosphate) extraction process, this dissolved radioactive iodine can escape from the solution as organic iodine compounds, such as methyl iodide.[113] Approximately 1–2% of the radioactive iodine forms insoluble iodides or iodates with palladium and silver among the fission products, presenting as fine particles in the dissolution solution and eventually being filtered out and concentrated.[114] These insoluble radioactive iodides are stored in temporary storage tanks or solidified with other high-level wastes; traces of radioactive iodine have also been found in the off-gas of the solidification process. Burger and Scheele *et al.*[115] summarized the distribution pathways of radioactive iodine in typical wet reprocessing plants for spent fuel.

### 3.4 Traditional capture techniques for radioactive iodine

The control of iodine involves removing as much iodine as possible from the dissolution solution into the off-gas stream, followed by its removal in the dissolution off-gas control system; this step is referred to as iodine stripping.[112] One relatively mature technique for removing gaseous iodine from the dissolution off-gas is caustic scrubbing. Caustic scrubbing is commonly used in the dissolution off-gas control systems of reprocessing plants such as the Hague reprocessing plant in France, the Windscale reprocessing plant in the UK, and the Rokkasho reprocessing plant in Japan.[99,115] However, caustic scrubbing is not effective in removing organic iodides. In the reprocessing of sodium-cooled fast reactors, high-concentration nitric acid is used to remove radioactive iodine from the off-gas, known as the Iodox process.[116,117] The strong oxidizing property of concentrated nitric acid effectively captures iodine vapor and organic iodides. However, the Iodox process requires additional steps for nitric acid concentration, nitric acid recovery, and waste treatment. Additionally, some reprocessing plants in the UK and the USA use the Mercurex process in their dissolution off-gas control systems to remove radioactive iodine.[104,116] Similar to the Iodox process, the Mercurex process uses a $Hg(NO_3)_2$–$HNO_3$ solution for scrubbing. The gaseous iodine is effectively absorbed by the solution, forming mercury iodate and iodide complexes. But the waste treatment issues associated with the Mercurex process limit its widespread application.

After acid scrubbing, trace amounts of radioactive iodine often remain in the off-gas, with levels exceeding safe radioactive limits. In such cases, additional methods, such as solid adsorption,[61] are needed to reduce the radioactive iodine concentration to below safe levels. Traditional methods using solid materials for capturing radioactive iodine, including activated carbon,[118] silver-based materials,[117] zeolites,[119] and metal oxides,[120] each have their own set of limitations despite being widely used. Activated carbon, known for its high surface area and porosity, physically adsorbs iodine through van der Waals forces.[118,121] However, its efficiency drops significantly in the presence of moisture or other competing gases, and regenerating or disposing of spent carbon, especially when heavily contaminated, is challenging.[122] Silver-based materials, such as silver-impregnated zeolites and filters, chemically react with iodine to form stable silver iodide, offering high efficacy.[123,124] But the high cost of silver, coupled with limited adsorption

Published on 02 mis Genver 2025. Downloaded on 06/02/2026 05:45:19.

capacity and non-regenerability, makes large-scale applications expensive.[123] Zeolites, which trap iodine through physical adsorption and ion exchange processes, suffer from moisture sensitivity, reduced selectivity in mixed gas environments, and difficulties in regeneration and maintaining structural integrity.[119,125,126] Similarly, metal oxides like manganese oxide and copper oxide chemisorb iodine, forming stable compounds, but face slow reaction kinetics, limited capacity, and challenges in regenerating without losing activity.[120,127] These significant drawbacks in traditional iodine capture methods underscore the need for advanced materials like covalent organic frameworks (COFs), which promise tunable properties and potentially superior performance in addressing the limitations of current technologies.

## 4 The intrinsic structure of COF

COFs are typical framework-type crystalline materials constructed by the extended connection of organic building blocks. Their intrinsic structure plays a crucial role in determining their iodine adsorption performance. Key structural features that enhance the effectiveness of COFs in iodine adsorption include porosity, conjugated structures, and hydrogen bonding.

### 4.1 Porosity

COFs possess highly ordered porous structures with fixed pore sizes and well-defined shapes. These pores provide ample surface area for iodine molecules to be adsorbed, thereby enhancing the overall adsorption capacity. Liu *et al.*[72] reported four different 2D COFs synthesized from one amine monomer and four aldehyde monomers, named Micro-COF-1, Micro-COF-2, Meso-COF-3, and Meso-COF-4 (as shown in Fig. 5(A)). The pore sizes of these COFs are 1.6 nm, 1.7 nm, 4.0 nm, and 4.7 nm, respectively, with increasing pore volumes accordingly. The $Q_e$ of the four COFs are 2.9 g g$^{-1}$, 3.5 g g$^{-1}$, 4.0 g g$^{-1}$, and 3.3 g g$^{-1}$, respectively. Experimental results indicate that when physical adsorption is predominant, pore volume and intrinsic pore size are decisive factors for the iodine adsorption performance of COFs. Jiang *et al.*[24] reported two 2D COFs with different topologies, TPB-DMTP [$C_3$ + $C_2$] and TTA-TTB [$C_3$ + $C_3$] (as shown in Fig. 5(B)). The differences in their topological structures result in different intrinsic pore sizes, 3.3 nm for TPB-DMTP and 2.2 nm for TTA-TTB. Structurally, both have continuous 1D channels without cross-linked pores and lack specific iodine adsorption sites. Relying solely on van der Waals forces for physical adsorption, TPB-DMTP exhibited an impressive iodine adsorption capacity with $Q_e$ of 6.2 g g$^{-1}$, which may be attributed to its large pore volume (1.28 cm$^3$ g$^{-1}$); TTA-TTB had a $Q_e$ of 5.0 g g$^{-1}$. This work demonstrated that high $Q_e$ could be achieved solely by utilizing the intrinsic pore structures of COFs without specific framework functionalization. However, the adsorption rate of TPB-DMTP was very low, at only 0.15 g g$^{-1}$ h$^{-1}$, requiring 100 hours to reach saturation.

Additionally, the pore sizes of COFs are tunable. During synthesis, the pore sizes can be controlled to precisely match the size of iodine molecules. Mi *et al.*[26] synthesized TP-PDA-COF and TP-BPDA-COF using 2,5-diaminopyridine and 5,5′-diaminobipyridine with 1,3,5-triformylphloroglucinol (Tp), and further quaternized the pyridine nitrogen with bromoethane to obtain ionic framework structures C-TP-PDA-COF and C-TP-BPDA-COF (as shown in Fig. 6(A)). The study found that

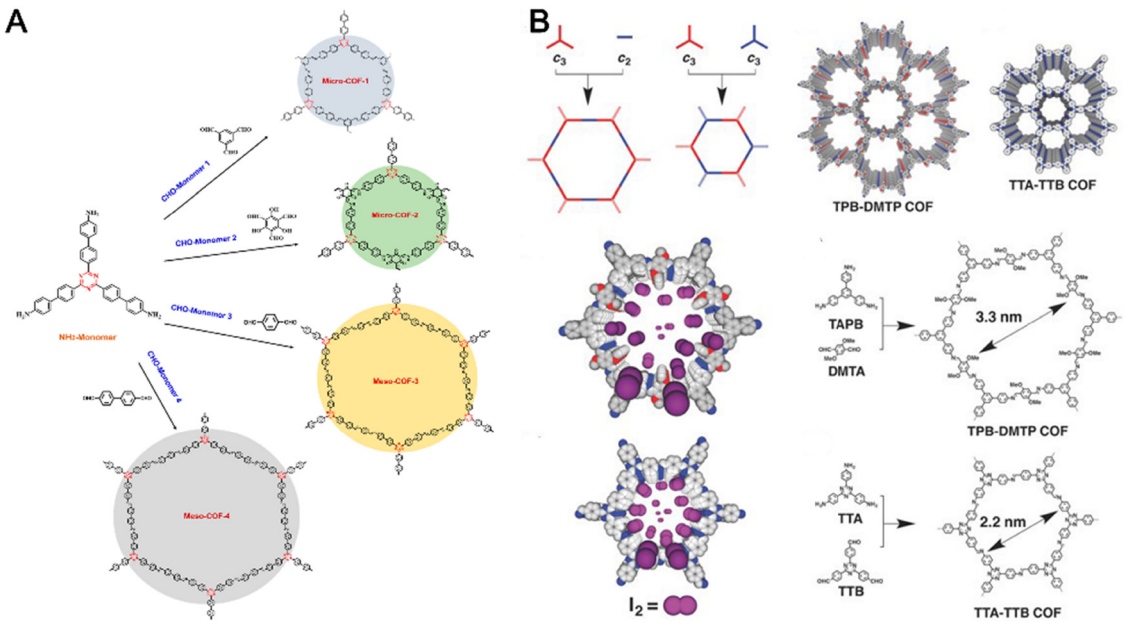


Fig. 5 By changing the monomer to regulate the pores of COF adsorbents. (A) The pore structure of Micro-COF-1, Micro-COF-2, Meso-COF-3, and Meso-COF-4. Reproduced with permission from ref. 72, Copyright©2019 American Chemical Society. (B) The pore structure of TPB-DMTP and TTA-TTB. Reproduced with permission from ref. 24, Copyright©2018 WILEY-VCH Verlag GmbH & Co.

 This journal is © The Royal Society of Chemistry 2025

Published on 02 mis Genver 2025. Downloaded on 06/02/2026 05:45:19.

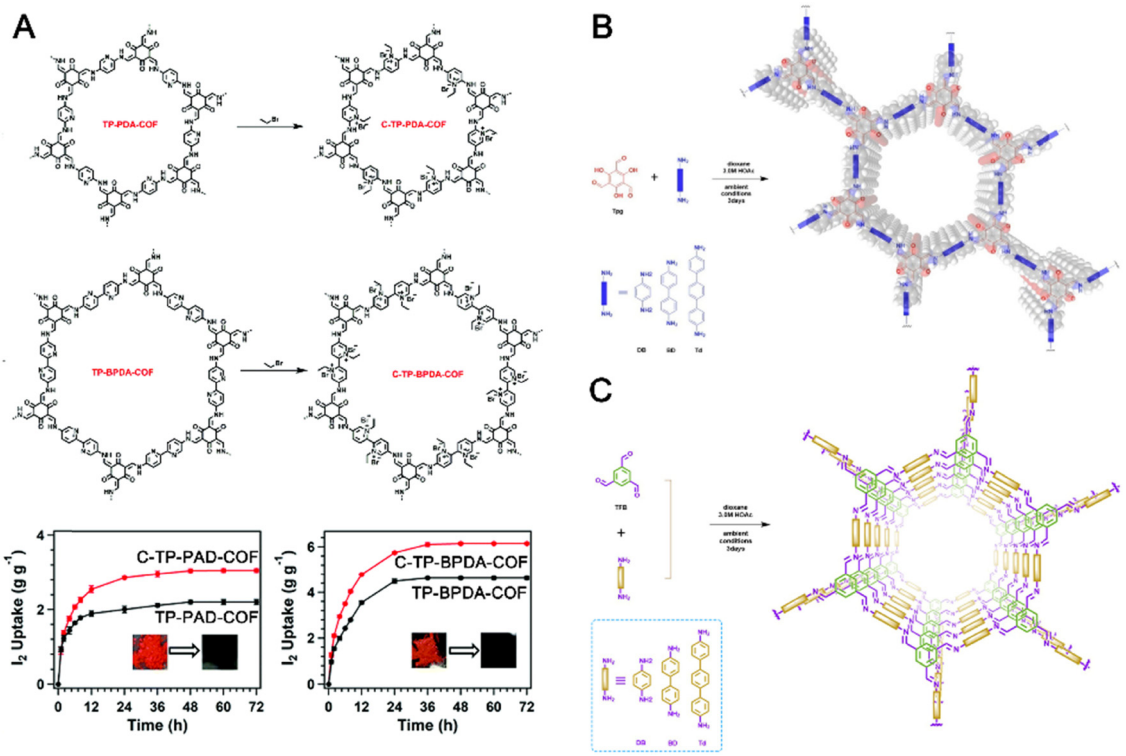


Fig. 6 Post-modification strategy and *de novo* synthesis strategy regulate the pore structure of COF adsorbents. (A) The structures and iodine adsorption curves of TP-PDA-COF, TP-BPDA-COF, C-TP-PDA-COF, and C-TP-BPDA-COF. Reproduced with permission from ref. 26. Copyright©2016 Royal Society of Chemistry. (B) The synthesis strategies of COF-TpDB, COF-TpBD, and COF-TpTd with different pores. Reproduced with permission from ref. 75. Copyright©2020 American Chemical Society. (C) Synthesis strategies for TFB-DB, TFB-BD, and TFB-Td with different pores (from ref.). Reproduced with permission from ref. 86. Copyright©2021 American Chemical Society.

C-TP-PDA-COF and C-TP-BPDA-COF, with similar pore structures, exhibited better adsorption performance; the ionic framework structure increased the COFs' $Q_e$ by 1.3 times. Electron cloud density analysis indicated that the strong electrostatic interaction between the positively charged pyridine and $I_2$ was the main reason for the enhanced adsorption performance. Among them, C-TP-BPDA-COF had the highest $Q_e$ of 6.1 g g$^{-1}$, but it took 72 hours to reach saturation. Wang *et al.*[75] studied the Tp-COF focusing on the relationship between the regulated pore size and the (physical) adsorption performance of iodine. As shown in Fig. 6(B), by varying the length of the amino monomers, the intrinsic pore sizes of the COFs were systematically controlled. The pore sizes of COF-TpDB, COF-TpBD, and COF-TpTd were 6.8 nm, 8.3 nm, and 9.9 nm, respectively. Their $Q_e$ were 2.75 g g$^{-1}$, 1.81 g g$^{-1}$, and 1.66 g g$^{-1}$, respectively, with saturation times of about 80 hours. Similarly, Liu *et al.*[86] investigated the adsorption properties of TFB-COF (TFB stands for 1,3,5-triformylbenzene) using the same amino monomers (DB, BD, and Td). In this study, TFB-DB, TFB-BD, and TFB-Td COFs reached adsorption saturation in 54 hours, with $Q_e$ of 6.40 g g$^{-1}$, 6.23 g g$^{-1}$, and 4.97 g g$^{-1}$, respectively. The pore sizes measured by BET method were 0.9 nm, 2.8 nm, and 3.4 nm, respectively. The differences in properties between Tp-COF and TFB-COF can be summarized as follows: (1) due to the enol–ketone tautomerism in Tp-COF, the enol-imine part of the Tp unit can convert to keto–enamine, reducing the π–π conjugation characteristic of the COF framework; (2) the adsorption in both types of COFs is primarily driven by weak interactions, and the limited range of these weak interactions means that excessively large pore sizes are not conducive to the occurrence of these interactions, resulting in reduced iodine desorption energy.

The tunability of COF pore sizes enhances their selectivity for iodine adsorption, preventing the adsorption of unwanted species. Although studies specifically on iodine-selective adsorption have not yet been reported, the potential of tunable pore-sized COFs as selective adsorption tools for gaseous iodine is undeniable. Ma *et al.*[128] reported the use of sub-nanoporous COFs for the separation of radioactive gases xenon (Xe) and krypton (Kr). They synthesized TFB-TAPA and TFP-TAPA with pore sizes of approximately 13 Å through aldehyde–amine condensation reactions. Further alkylation adjusted the sub-nanopores to produce TFB-TAPA-Bu and TFP-TAPA-Bu with pore sizes of approximately 7 Å. The resulting 7 Å sub-nanopores, slightly larger than the dynamic diameters of Xe/Kr, endowed the COFs with effective adsorption and separation capabilities for these gases. The maximum adsorption capacity for Xe reached 85.6 cm$^3$ g$^{-1}$, and the selectivity for Xe over Kr was up to 9.7.

In addition, the interlayer stacking structure of 2D COFs directly influences their pore channels, with stacking modes including AA, AB, and ABC. Taking imine COFs as an example,

Published on 02 mis Genver 2025. Downloaded on 06/02/2026 05:45:19.

the same reactants can yield three COF isomers with different stacking structures (overlapping AA, staggered AB, and ABC stacking) under varying reaction temperatures and solvent environments. Experimental and theoretical studies show that the ABC-stacked isomer obtained at room temperature is a kinetic product, while the AA-stacked isomer prepared *via* solvothermal methods is a thermodynamic product.[129] The differences in stacking modes arise from inconsistent tautomeric configurations, which, in turn, lead to variations in their efficiencies for generating type I and type II reactive oxygen species (ROS). Furthermore, the spatial steric hindrance of the building blocks is a key factor influencing the stacking modes.[130] Although research on the impact of COF stacking modes on iodine adsorption is limited, future studies should consider this aspect to improve adsorption performance.

### 4.2 Conjugated structures

Two-dimensional COFs are stacked through π–π interactions and van der Waals forces, making their conjugated π-electron systems an intrinsic structural feature.[37] This conjugated π-electron system can enhance interactions with iodine molecules, significantly increasing the adsorption affinity and capacity of COFs for iodine. Shui *et al.*[81] reported two fully conjugated COFs synthesized from 4,4′,4″,4‴-(pyrene-1,3,6,8-tetrayl)tetrabenzaldehyde (PyTTA) and 1,2,4,5-tetrakis(4-formylphenyl)benzene (TFPB), resulting in TFPB-PyTTA-COF and TFPB-BPTA-COF (Fig. 7(A)). Their study found that both COFs primarily utilize physical adsorption combined with some chemical adsorption. The pyrene-containing TFPB-PyTTA-COF exhibited a higher $Q_e$ (5.6 g $g^{-1}$) than TFPB-BPTA-COF (4.0 g $g^{-1}$). This difference is likely due to the larger π–π conjugation area provided by the pyrene units in PyTTA compared to the benzene units in TFPB.

Luo *et al.*[78] investigated the differences in static iodine adsorption between the fully π–π conjugated COF-LZU1 and COF-TpPa, which features both π–π and p–π conjugated structures. COF-LZU1 demonstrated a higher iodine adsorption capacity than COF-TpPa. XPS and Raman spectroscopy studies confirmed that COF-TpPa's adsorption was entirely driven by van der Waals forces and involved no iodine species other than $I_2$. In contrast, COF-LZU1's adsorption was a combination of physical and chemical adsorption, where the physical adsorption was attributed to the intrinsic pores of COF-LZU1 and the chemical adsorption to its fully π–π conjugated structure. Zeng *et al.*[85] reported two π–π conjugated two-dimensional COFs, TJNU-201 and TJNU-202 (Fig. 7(B)), which exhibited excellent iodine adsorption capacities through combined physical and chemical adsorption mechanisms, with $Q_e$ of 5.6 g $g^{-1}$ and 4.8 g $g^{-1}$, respectively. The superior adsorption capacity of TJNU-201 compared to TJNU-202 is likely due to its higher nitrogen content. Jiang *et al.*[131] reported a hierarchically porous covalent triazine framework, CTF-CTTD, which featured abundant pore channels, triazine units, and a π–π conjugated structure, resulting in an iodine adsorption capacity of 3.8 g $g^{-1}$.

### 4.3 Hydrogen bonds

COFs can undergo noncovalent interactions to introduce additional adsorption sites. These noncovalent interactions can form strong interactions with iodine,[132,133] such as hydrogen bonds or halogen bonds, further enhancing the adsorption capacity, rate and selectivity of COFs. Hydrogen-bonded cross-linked organic frameworks, which are rich in hydrogen bond structures, are a prominent example of this approach.

Ke *et al.*[134] developed a crystalline microporous hydrogen-bonded cross-linked organic framework, HCOF-1, using a light-induced assembly and single-crystal-to-single-crystal transformation strategy

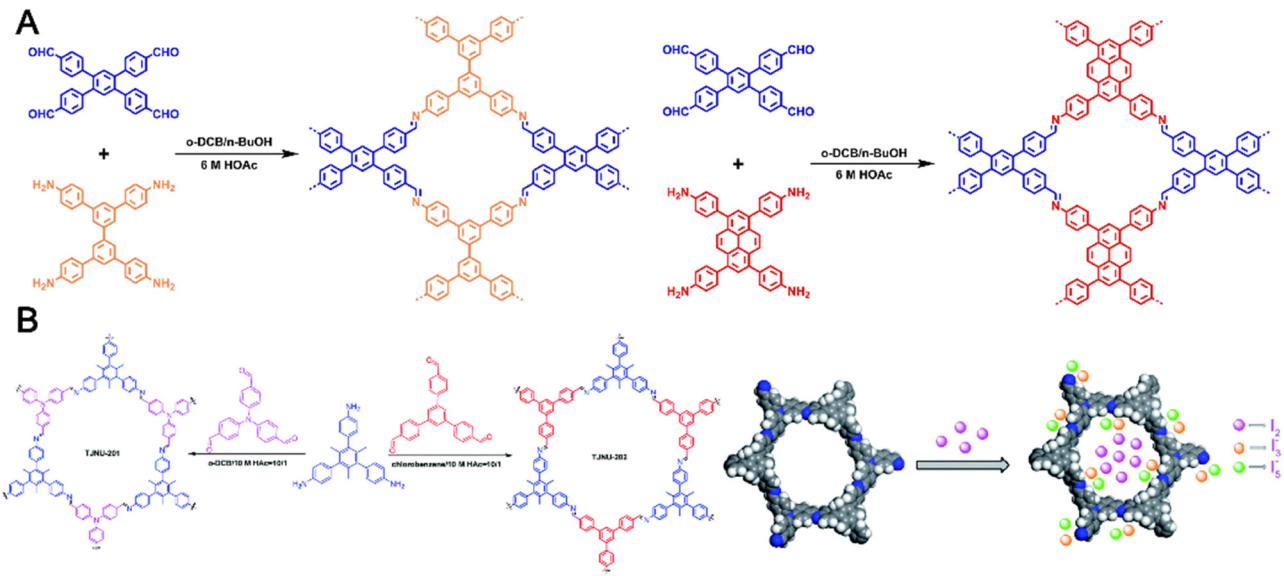


Fig. 7 The typical conjugated structure COF adsorbents. (A) The synthesis of TFPB-PyTTA-COF and TFPB BPTA COF with conjugated structures. Reproduced with permission from ref. 81. Copyright©2022 Wiley-VCH GmbH. (B) Synthesis and iodine adsorption mechanism of TJNU-201 and TJNU-202 with conjugated structures. Reproduced with permission from ref. 85. Copyright©2020 Royal Society of Chemistry.

 This journal is © The Royal Society of Chemistry 2025

Published on 02 mis Genver 2025. Downloaded on 06/02/2026 05:45:19.

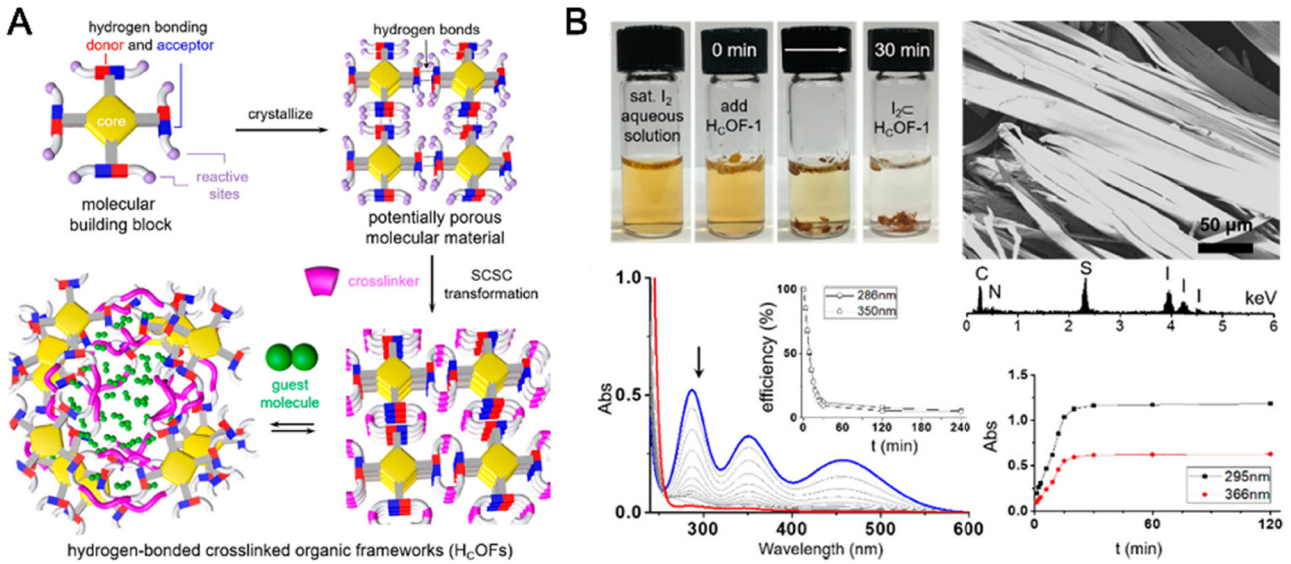


Fig. 8 Microporous hydrogen bonded cross-linked organic framework HCOF-1 and its adsorption of iodine. Reproduced with permission from ref. 134. Copyright©2017 American Chemical Society.

(Fig. 8). In this system, ethane dithiol acts as a cross-linking agent, forming C–S bonds between two alkyne groups. HCOF-1 can rapidly adsorb $I_2$ in an aqueous system with a high adsorption capacity of 290 wt%, primarily due to the formation of N–H···I hydrogen bonds and N···I and S···I halogen bonds with $I_2$ molecules. The highly elastic framework of HCOF-1 allows its pores to expand spatially, not only providing high iodine adsorption capacity but also excellent recyclability, enabling it to return to its original crystalline form after desorbing iodine. Amide groups, capable of forming infinite stacked structures through hydrogen bonding, are advantageous in designing hydrogen-bonded organic frameworks. Claverie *et al.*[135] synthesized a series of HOFs with 1D, 2D, or 3D hydrogen-bonded frameworks using benzene-1,3,5-tricarboxamide and amide-containing tribenzoic monomer as building blocks. Their study showed that three porous HOFs, HOF-B-Hex, HOF-T-Pr, and HOF-T-Hex, exhibited permanent porosity, demonstrating the effectiveness of the amide-based HOF synthesis strategy. Among them, HOF-T-Hex stood out with a pore volume of 42% and a gas-phase iodine capture capacity of 6.4 g $g^{-1}$. The iodine capture capacity of HOFs is influenced not only by pore volume but also by the surplus π-electrons in the material, which do not participate in π–π stacking interactions.

In summary, the intrinsic structures of COFs, including their tunable porous structures, π-electron conjugated systems, and hydrogen-bonding frameworks, or their synergistic interactions, contribute to their excellent performance in iodine adsorption applications. These structural features enable COFs to effectively capture and retain iodine molecules, making them highly promising materials for nuclear industry off-gas treatment.

## 5 Functionalization of COFs

Under conventional static adsorption conditions, most COFs have equilibrium adsorption times that span tens to hundreds of hours, which may not meet the requirements for capturing radioactive iodine from off-gas streams. Reported 2D COFs often prioritize high $Q_e$, overlooking the adsorption rate. In addition to $Q_e$, $k_{80\%}$ is an important metric to consider. Ma *et al.*[64] first proposed the metric $k_{80\%}$ to describe the adsorption rate of COF-based iodine adsorbents. The $k_{80\%}$ value, defined as the average adsorption rate when reaching 80% of the $Q_e$, has gained widespread recognition and application among researchers in the field. Therefore, improving the $k_{80\%}$ of COFs while maintaining $Q_e$ is a critical scientific challenge in this area.

Rational design of COF structures is crucial in addressing this issue. Physical adsorption typically depends on the pore volume, pore size, and the cross-linking manner of the pore channels in COFs,[136,137] leading to long times to reach adsorption equilibrium. A current viewpoint suggests that combining physical and chemical adsorption, or prioritizing chemical adsorption, by introducing active adsorption sites is an effective strategy to improve both saturation capacity and adsorption rate.[138] Electron-rich groups containing heteroatoms, such as C=N, $-NH_2$, N–H, triazine, pyridine, tetrathiafulvalene, sulfur- or phosphorus-containing heterocycles, can serve as active adsorption sites.[139–141] The lone pairs on heteroatoms can transfer to the σ* antibonding orbital of iodine to form charge-transfer complexes.[57] The partial negative charge on the iodine atoms due to this electron transfer facilitates the formation of polyiodide ions, which are then fixed in place. The same electron-rich group can exhibit significantly different iodine affinities depending on the COF framework or the adjacent connecting units.[66] During chemical adsorption, the electron-rich groups on the COF framework interact with $I_2$, promoting the transformation of adsorbed $I_2$ in the COF channels into polyiodide ions such as $I_3^-$ and $I_5^-$.[63,64] This chemical interaction helps enhance both the adsorption

Published on 02 mis Genver 2025. Downloaded on 06/02/2026 05:45:19.

capacity and rate. This concept has been validated in numerous design and synthesis cases of COF-based iodine adsorbents.

### 5.1 Electron-rich COFs

Building blocks containing heteroatoms (N, S, O, P, *etc.*) can endow COFs with local electron-rich characteristics, thereby enhancing iodine adsorption capacity. Dong *et al.*[83] synthesized two COFs using monomers containing tetrathiafulvalene components, namely, the 2D TTF-TD-COF and the 3D TTF-TAPT-COF (as shown in Fig. 9(A)). Both COFs exhibit a combination of physical and chemical adsorption for iodine, with $Q_e$ of 4.3 g g$^{-1}$ and 5.0 g g$^{-1}$, and $k_{80\%}$ values of 0.39 g g$^{-1}$ h$^{-1}$ and 0.51 g g$^{-1}$ h$^{-1}$, respectively. Fang *et al.*[89] reported two tetrathiafulvalene-based COFs, JUC-560 and JUC-561 (as shown in Fig. 9(B)), where the former is a 2D COF and the latter a 3D COF. The results indicate that the synergy between physical and chemical adsorption grants JUC-560 and JUC-561 high $Q_e$ and $k_{80\%}$, with capacities of 5.2 g g$^{-1}$ and 8.1 g g$^{-1}$, and $k_{80\%}$ of 0.49 g g$^{-1}$ h$^{-1}$ and 0.70 g g$^{-1}$ h$^{-1}$, respectively. JUC-560 and JUC-561 are designed with large specific surface areas, effectively enhancing the physical adsorption process within COF channels. Additionally, the tetrathiafulvalene groups, rich in sulfur heteroatoms, serve as chemical adsorption sites on the COF framework. The electron-rich groups interact with $I_2$, facilitating the transformation of $I_2$ into polyiodide ions such as $I_3^-$ and $I_5^-$, thereby improving the $k_{80\%}$ of JUC-560 and JUC-561. This combination of physical and chemical interactions significantly boosts both the adsorption capacity and rate, demonstrating the effectiveness of incorporating electron-rich heteroatom groups in COF structures for iodine capture.

Chen *et al.*[27] reported the grafting of Povarov reaction products onto TPB-DMTP-COF. By utilizing the electron-rich ethynyl groups of *para*-ethynylbenzene and the imine portions of TPB-DMTP, an electrophilic aromatic substitution cyclization reaction generated a COF containing quinoline structures, named COF-PA. The conversion of imine bonds to rigid quinoline structures significantly enhanced the chemical stability of COF-PA. It maintained its crystallinity and crystal structure after seven days in strong acidic (12 M HCl) and alkaline (14 M NaOH) environments as well as in organic solvents. The introduction of electron-rich ethynyl and quinoline groups facilitated chemical interactions between these groups and iodine. XPS and Raman spectroscopy confirmed that during the adsorption process, electrons transferred from the electron-rich quinoline to the electron-deficient $I_2$, and the ethynyl sites also participated in chemical adsorption of $I_2$. Although this modification sacrificed some specific surface area and pore size, it resulted in a significant improvement in iodine adsorption performance, with a $k_{80\%}$ value of 1.30 g g$^{-1}$ h$^{-1}$ and a $Q_e$ of 4.5 g g$^{-1}$. Lin *et al.*[88] synthesized two COFs, PB-TT-COF and PA-TT-COF, using an aldehyde monomer containing benzothiophene with tris(4-aminophenyl)benzene (PB) and tris(4-aminophenyl)amine (PA), respectively. The $Q_e$ of PB-TT-COF was 5.9 g g$^{-1}$, while that of PA-TT-COF was 5.1 g g$^{-1}$. The planar

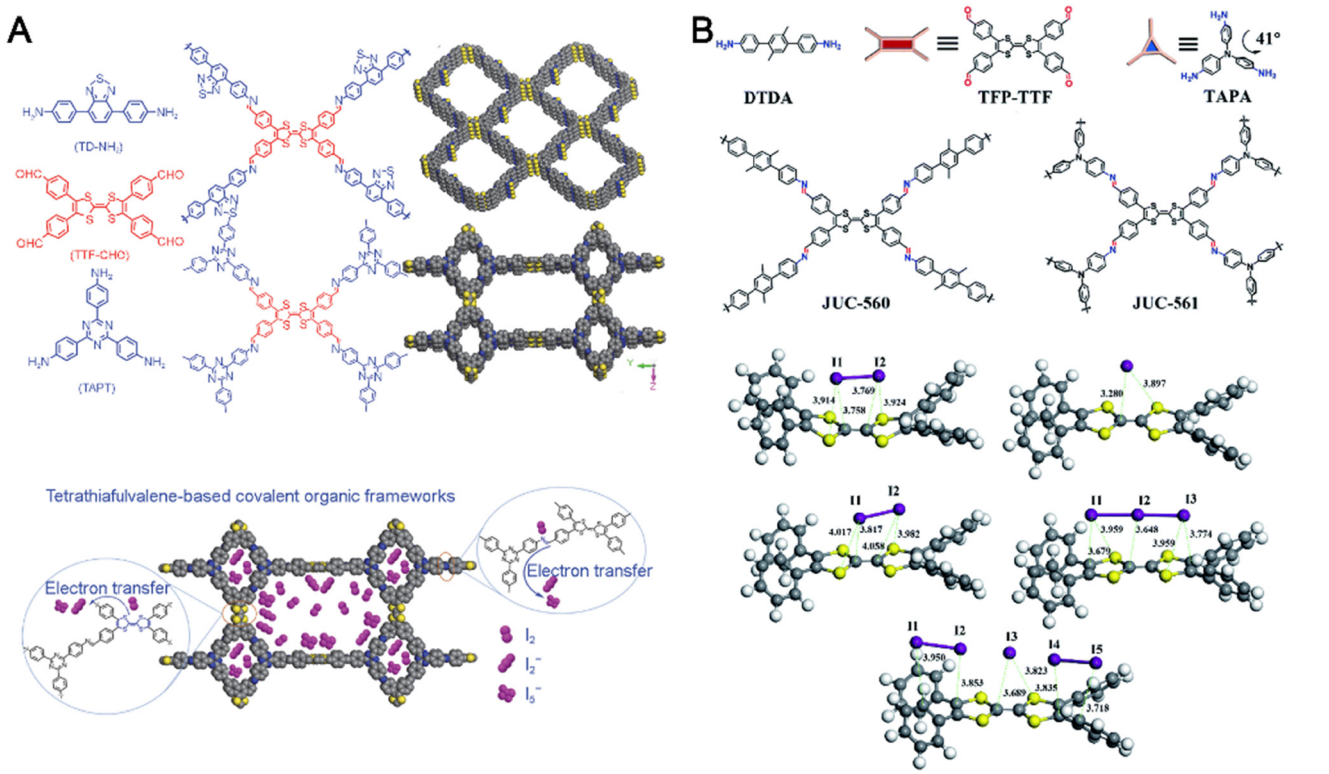


Fig. 9 Tetrathiofulvalene-based COF adsorbents. (A) The chemical structure and adsorption mechanism of TTF-TD-COF and TTF-TAPT-COF. Reproduced with permission from ref. 83. Copyright©2022 Springer Nature. (B) Chemical structure and adsorption mechanism of JUC-560 and JUC-561. Reproduced with permission from ref. 89. Copyright©2021 Royal Society of Chemistry.

 This journal is © The Royal Society of Chemistry 2025

Published on 02 mis Genver 2025. Downloaded on 06/02/2026 05:45:19.

conjugated structure of PB contrasted with the trigonal pyramidal shape of PA, resulting in significant differences in morphology and specific surface area between PB-TT-COF and PA-TT-COF. Despite the reduced specific surface area, the sheet-like structure of PA-TT-COF endowed it with faster adsorption rates and superior adsorption capacities in cyclohexane solution, approximately 2.4 times that of PB-TT-COF. This research inferred that the sheet-like structure created a more abundant external surface, allowing adsorption sites on this surface to more rapidly interact with and adsorb the $I_2$, compared to the benzothiophene (chemical) adsorption sites within the pores, resulting in an enhancement in adsorption rates.

Nitrogen-rich COFs have garnered significant attention in the field of iodine adsorption, primarily due to the high chemical affinity of units like C=N and nitrogen-containing aromatic rings for iodine. However, the correlation between the heteroatoms in the chemical environment of COF frameworks and their iodine adsorption performance has not been fully elucidated. Li *et al.*[87] synthesized a stable nitrogen-rich TAPA-PDA COF, which demonstrated high efficiency and reversibility in gaseous iodine capture, with an adsorption capacity of 5.0 g $g^{-1}$. The study found that the high density of *N*-iodophilic sites uniformly distributed on the pore surfaces of TAPA-PDA-COF facilitated efficient iodine capture. Enhancing the density of electron-rich moieties to strengthen specific host–guest interactions during adsorption is a novel COF design strategy. Wang and Han *et al.*[63] introduced bipyridine building blocks to synthesize the nitrogen-rich SCU-COF-2 (as shown in Fig. 10(A)). Based on the enhanced electron pair effect, SCU-COF-2 can capture both iodine and iodomethane. Under static adsorption conditions, SCU-COF-2 exhibited an $Q_e$ of 6.0 g $g^{-1}$ with a saturation time of 96 hours, and an iodomethane adsorption capacity of 1.45 g $g^{-1}$. DFT calculations indicated that during adsorption, iodine tends to occupy positions near the nitrogen atoms on the pyridine rings within the hexagonal channels, forming charge-transfer complexes through interactions with multiple nitrogen atoms, which is the primary adsorption mechanism.

Ma and Li *et al.*[82] designed multi-nitrogen nodes to construct a series of COFs with dual channels and tertiary amine active sites, including TAPD-PDA, TAPD-DMTA, and TAPD-DHTA (as shown in Fig. 10(B)). The nitrogen atom counts per repeating unit reached up to six, providing the COFs with excellent iodine adsorption performance, with capacities of 5.09 g $g^{-1}$, 5.54 g $g^{-1}$, and 4.02 g $g^{-1}$, respectively. Adsorption experiments combined with DFT theoretical calculations confirmed that the adsorption affinity of nitrogen sites in COFs can be further modulated by introducing different electron-donating groups. Introducing $-OCH_3$ can increase the electron cloud density near nitrogen active sites *via* the inductive effect, thereby enhancing binding energy with iodine. Conversely, –OH tends to form intramolecular hydrogen bonds with adjacent imine groups, reducing the electron density around the

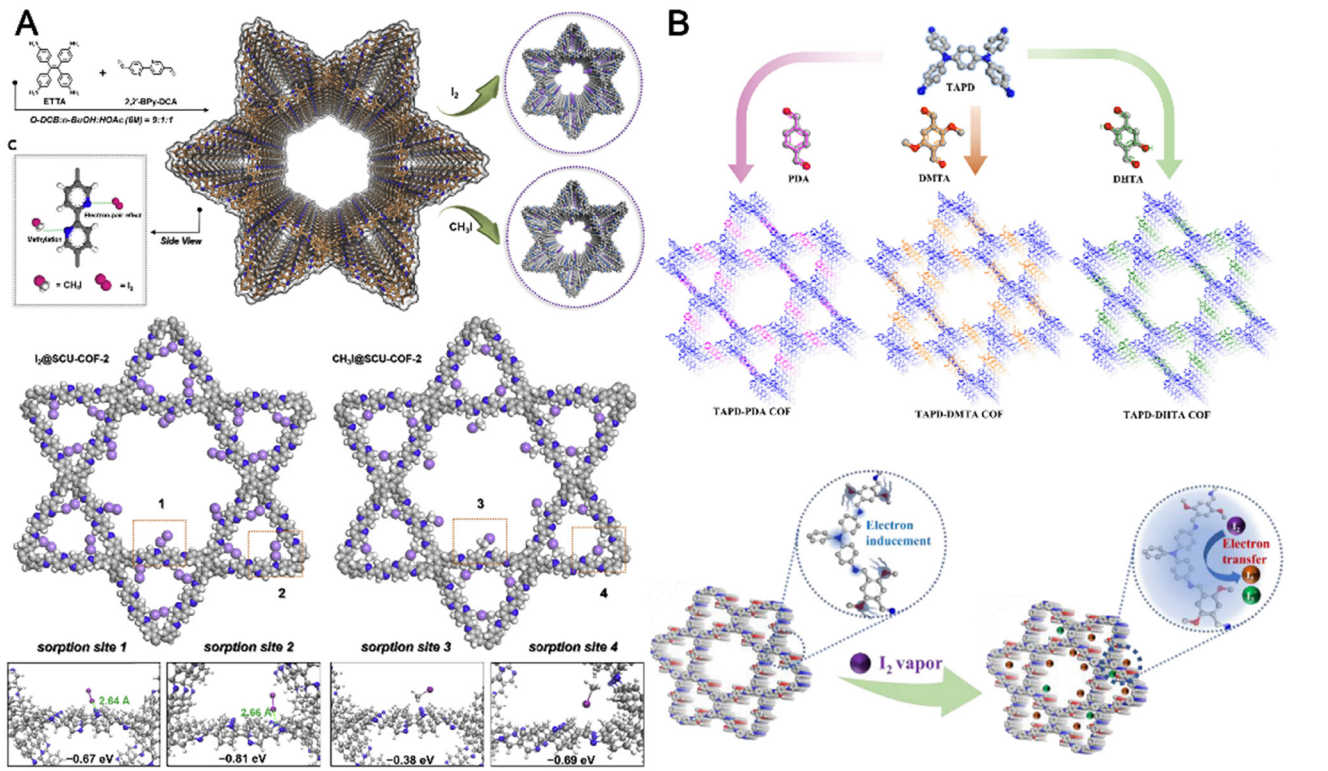


Fig. 10 Design and synthesis of COF adsorbents using nitrogen enrichment strategies. (A) Preparation of SCU-COF-2 and its adsorption mechanism for iodine and iodomethane. Reproduced with permission from ref. 63. Copyright©2020 Elsevier Inc. (B) Synthesis of TAPD-PDA, TAPD-DMTA, and TAPD-DHTA and their mechanism for iodine capture. Reproduced with permission from ref. 82. Copyright©2022 Elsevier Inc.

Published on 02 mis Genver 2025. Downloaded on 06/02/2026 05:45:19.

nitrogen sites, ultimately decreasing iodine adsorption capacity. The phenomenon of intramolecular hydrogen bond suppression within the framework was also observed by Zeng *et al.*,[59] who reported two 2D COFs, TJNU-203 and TJNU-204, constructed from 1,3,5-trimethyl-2,4,6-tris(4-aminophenyl)benzene blocks with spatial distortion characteristics. TJNU-204, being an –OH functionalized version of TJNU-203, showed a lower adsorption capacity (5.3 g $g^{-1}$) compared to TJNU-203 (5.8 g $g^{-1}$), attributed to the formation of intramolecular hydrogen bonds between –OH groups and adjacent imine groups.

Fully elucidating the construction mechanism of regular pores in COFs and enhancing the density of adsorption sites while maintaining high iodine affinity and adsorption rates are crucial for developing high-performance COF adsorbents. Cheng *et al.*[74] synthesized BTT-TAPT-COF using nitrogen-rich and sulfur-rich units. Despite having abundant sulfur and nitrogen sites and an extended π–π conjugated structure, BTT-TAPT-COF exhibited an adsorption capacity of only 2.76 g $g^{-1}$. This was attributed to the competitive interactions among the electron-rich atoms, where the high-density uniform distribution of these atoms in the conjugated structure reduced their individual electron cloud density. Zhang *et al.*[34] reported a series of nitrogen/sulfur-rich COFs derived from porous organic cages (as shown in Fig. 11(A)), with COF USTB-1c demonstrating the highest iodine adsorption performance at 5.8 g $g^{-1}$. Mechanistic studies indicated that the binding energies of $I_3^-$ and $I_5^-$ with bipyridine units were −7.47 and −11.45 kcal $mol^{-1}$, respectively, compared to −6.92 and −11.14 kcal $mol^{-1}$ with bithiophene units. These results suggest that nitrogen atoms have a superior iodine capture capability compared to sulfur atoms. Cai *et al.*[70] employed a selective adsorption site synthesis strategy (as shown in Fig. 11(B)) and designed a novel monomer, 2-aminoterephthalohydrazide ($NH_2$-Th), which contains both amino and hydrazide units. This monomer was reacted with benzene-1,3,5-tricarbaldehyde to produce COF $NH_2$-Th-Bta. Compared to the non-amino functionalized counterpart COF Th-Bta, which had an iodine adsorption capacity of 0.68 g $g^{-1}$, $NH_2$-Th-Bta showed a significantly enhanced capacity of 3.58 g $g^{-1}$.

Luo *et al.*[67] reported the synthesis of quinazolinone-based COFs using an *in situ* photocatalytic reduction and cyclization post-modification strategy (Fig. 12(A)). Initially, two COFs with independent vinyl groups, ECUT-COF-10 based on benzene and ECUT-COF-12 based on triazine, were synthesized as structural analogs. The *in situ* photocatalytic reduction and cyclization of vinyl groups with adjacent aminobenzamide in the COF structure generated quinazolinone, resulting in ECUT-COF-11 and ECUT-COF-13. The modification with quinazolinone units expanded the 2D π–π conjugated network within the COF structure and significantly increased its nitrogen content, endowing the COF with electron-rich characteristics. Quinazolinone-based COFs showed marked improvements in both $Q_e$ and $k_{80\%}$. The $Q_e$ were as follows: ECUT-COF-13 (10.81 g $g^{-1}$) > ECUT-COF-12 (7.85 g $g^{-1}$) > ECUT-COF-11 (5.62 g $g^{-1}$) > ECUT-COF-10 (4.23 g $g^{-1}$). The $k_{80\%}$ values were: ECUT-COF-13 (1.4 g $g^{-1}$ $h^{-1}$) > ECUT-COF-12 (0.60 g $g^{-1}$ $h^{-1}$) > ECUT-COF-11 (0.45 g $g^{-1}$ $h^{-1}$) > ECUT-COF-10 (0.28 g $g^{-1}$ $h^{-1}$).

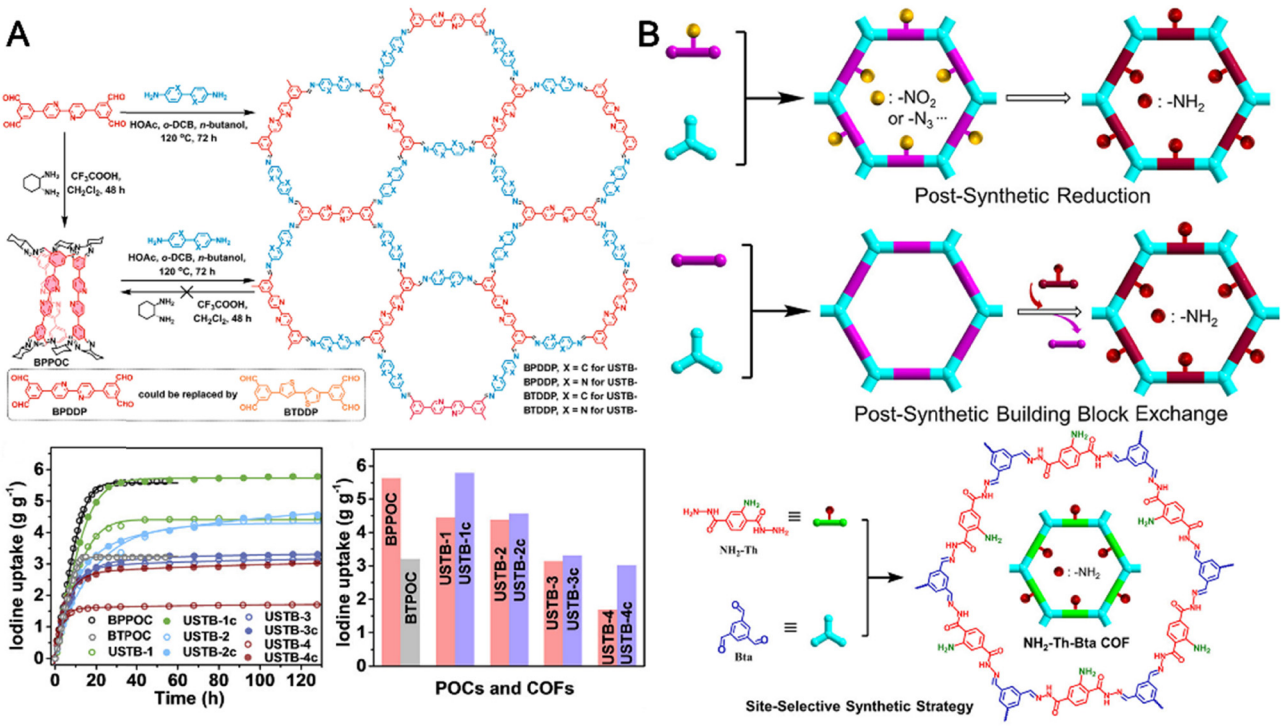


Fig. 11 Synthesis of COF adsorbents containing nitrogen/sulfur sites. (A) Rich nitrogen/sulfur COFs prepared by the transformation of nitrogen/sulfur porous organic molecular cages. Reproduced with permission from ref. 34. Copyright©2022 American Chemical Society. (B) Site-selective synthesis of amino functionalized $NH_2$-Th-Bta COFs at adsorption sites. Reproduced with permission from ref. 70. Copyright©2021 American Chemical Society.

 This journal is © The Royal Society of Chemistry 2025

Published on 02 mis Genver 2025. Downloaded on 06/02/2026 05:45:19.

Han *et al.*[25] investigated the adsorption of iodine and methyl iodide using nitrogen-rich COFs. They synthesized COF-TAPB and COF-TAPT by reacting tris(4-formylphenyl)amine (TFPA) with 1,3,5-tris(4-aminophenyl)benzene (TAPB) and 2,4,6-tris(4-aminophenyl)-1,3,5-triazine (TAPT), respectively (Fig. 12(B)). These COFs are structural analogs with identical crystal structures and textural properties, differing only in nitrogen content, making them ideal for studying nitrogen's role in adsorption. Studies on iodine adsorption showed that COFs provided multiple types of electron-donor sites, including triazine, imine, $sp^3$-N, and aromatic rings. Iodine could be relatively easily adsorbed at these sites through the formation of charge-transfer complexes and polyiodides. The properties of adsorption sites and pore structure characteristics influenced iodine adsorption. For methyl iodide adsorption, the process mainly involved *N*-methylation reactions at nucleophilic N sites, and the adsorption capacity was positively correlated with the distribution of strong binding sites. This adsorption mechanism is more favorable for capturing organic iodine at low concentrations. The static adsorption capacities of COF-TAPB and COF-TAPT for iodine were 7.9 g $g^{-1}$ and 8.6 g $g^{-1}$, respectively, with $k_{80\%}$ of 0.33 g $g^{-1}$ $h^{-1}$ and 0.48 g $g^{-1}$ $h^{-1}$, respectively. Additionally, the study found that ionic groups strongly enhanced iodine adsorption, though they had a less pronounced effect on methyl iodide adsorption.

### 5.2 Flexible COFs

Flexible COFs offer greater flexibility and adaptability compared to traditional COFs, characterized by their self-adaptive dynamic structural regulation.[142] This trait enables flexible COFs to adjust pore size and shape in response to environmental changes such as temperature and solvents.[143] During iodine adsorption, flexible COFs can adjust their pores to match the size of guest molecules, thereby achieving more efficient adsorption.

Ma *et al.*[65] were the first to report a series of flexible framework COFs synthesized using formic acid and the Eschweiler–Clarke reaction (as shown in Fig. 13(A)). Formic acid serves both catalytic and reductive roles, not only catalyzing the formation of rigid C=N bonds (typically achieved using acetic acid) in COF synthesis but also reducing them to flexible C–N bonds. The study found that flexible FAL-COF-1 had a higher $Q_e$ (5.4 g $g^{-1}$) compared to the rigid RIL-COF-1 (4.9 g $g^{-1}$), although FAL-COF-1 exhibited lower $k_{80\%}$ value. The increased adsorption capacity of FAL-COF-1 is attributed to its flexible framework, which can adapt during the adsorption of guest molecules. Chen *et al.*[77] reported two examples of flexible 2D COFs based on nitrogen-rich flexible building blocks, 2,4,6-tris(4-formylphenoxy)-1,3,5-triazine, namely TPT-azine-COF and TPT-TAPB-COF. The iodine adsorption capacities of these COFs were 2.19 g $g^{-1}$ and 2.25 g $g^{-1}$, respectively.

Dinari *et al.*[76] compared iodine adsorption between flexible amine-linked COFs and rigid imine-linked COFs. They synthesized Hz-COF with a rigid C=N structure using 2,4,6-tris(4-formylphenoxy)-1,3,5-triazine (TPT) and hydrazine, and then reduced it with $NaBH_4$ to create NH-COF with a flexible C–N structure. Adsorption experiments showed that NH-COF had a

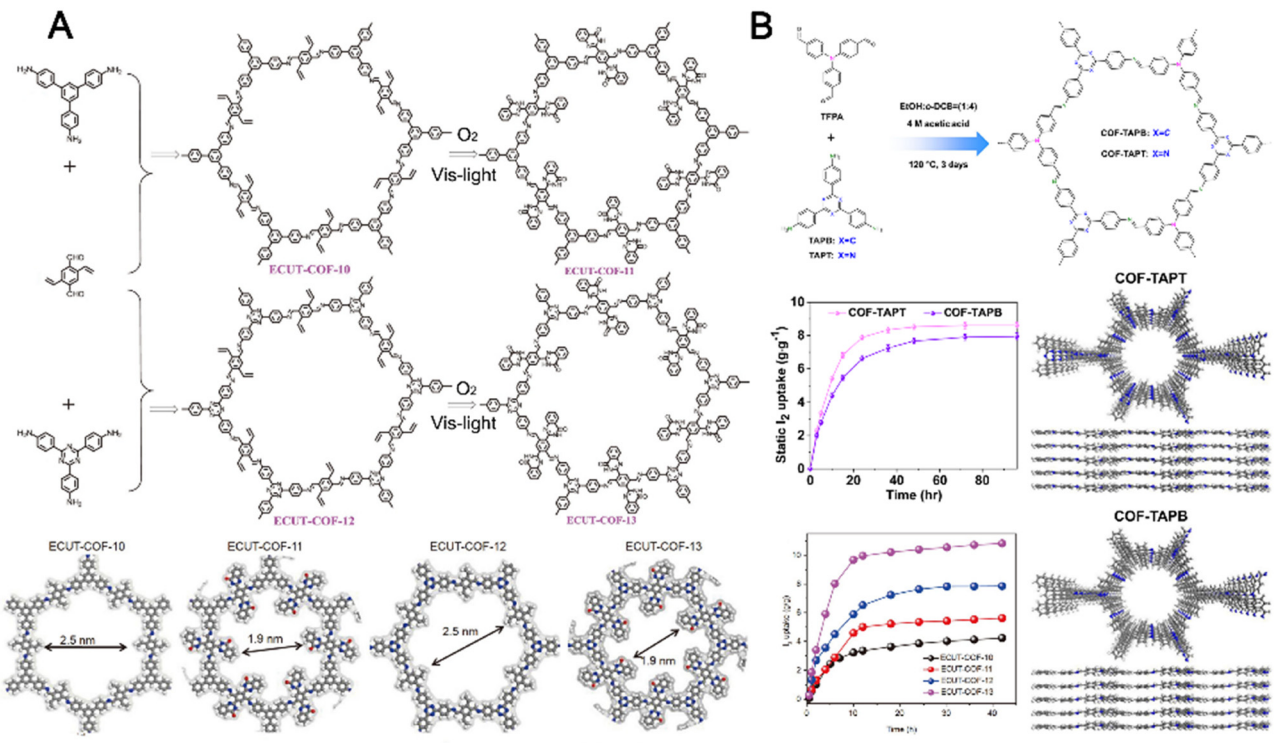


Fig. 12 High-performance electron-rich heteroatom functionalized COF adsorbents. (A) Preparation of quinolone-based COFs using *in situ* photocatalytic reduction cyclization strategy and their adsorption of iodine. Reproduced with permission from ref. 67. Copyright©2023 Springer Nature. (B) Construction of nitrogen rich COF-TAPB and COF-TAPT and their adsorption of iodine. Reproduced with permission from ref. 25. Copyright©2022 Springer Nature.

Published on 02 mis Genver 2025. Downloaded on 06/02/2026 05:45:19.

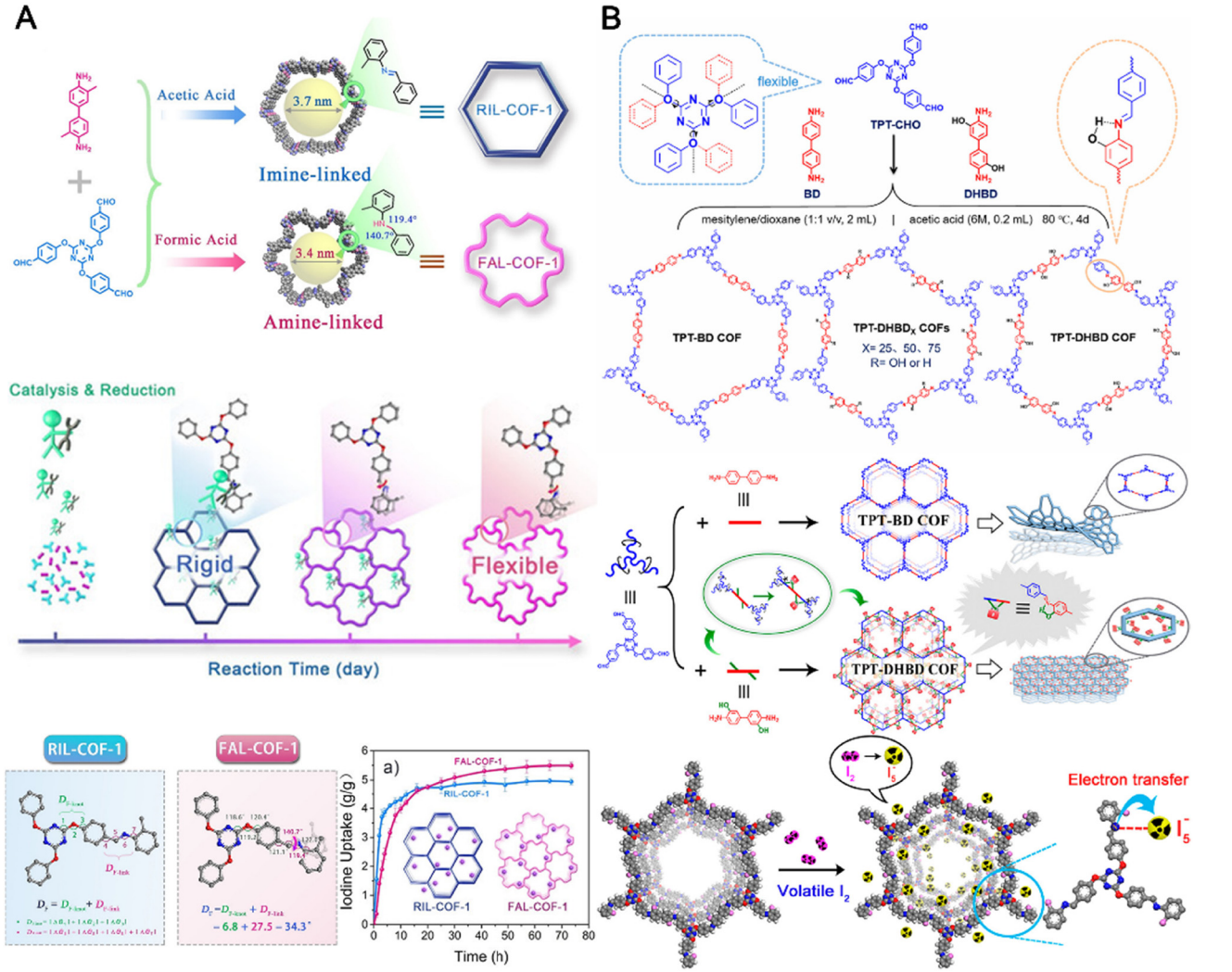


Fig. 13 Flexible COF adsorbents. (A) Using the Eschweiler–Clarke reaction to transform COFs from rigid to flexible, and their degree of flexibility and iodine adsorption curve. Reproduced with permission from ref. 65. Copyright©2021 Wiley-VCH GmbH. (B) Using hydrogen bonding to stabilize the flexible skeleton, transforming COFs from flexible to rigid, and their iodine adsorption mechanism. Reproduced with permission from ref. 80. Copyright©2018 American Chemical Society.

higher $Q_e$ (2.6 g g$^{-1}$) compared to Hz-COF (2.0 g g$^{-1}$) and exhibited better adsorption rates. The flexibility of the NH-COF framework and its N–H groups, which can form strong hydrogen bonds with iodine (N–H···I), contribute to its superior iodine capture performance. Guo *et al.*[80] reported the stabilization of flexible TPT units with hydrogen bonds to enhance the microstructural order and crystallinity of flexible imine-linked COFs (as shown in Fig. 13(B)). They discovered that controlling the hydrogen bond content in COFs could effectively regulate crystallinity. However, they found that iodine adsorption performance decreased with increasing hydrogen bond content. Since the hydrogen bonds form between nitrogen atoms in the imine linkages and hydrogen atoms on adjacent hydroxyl groups, it is inferred that nitrogen atoms in the imine linkages play a crucial role in effective iodine adsorption and conversion. Ke *et al.*[73] reported a flexible non-planar phosphine-based COF, P-COF. The unique microspherical morphology of P-COF endowed it with a high specific surface area (1056 m$^2$ g$^{-1}$). Its abundant nitrogen and phosphorus adsorption sites, along with an extensive π–π conjugated framework, contributed to a high iodine adsorption capacity of 6.19 g g$^{-1}$.

### 5.3 Ionic COFs

Incorporating ionic groups into COF structures to create ion-functionalized COFs can significantly enhance iodine adsorption performance through Coulomb interactions, which induce the formation of strong hydrogen bonds or halogen bonds and charge transfer complexes, converting iodine molecules into polyiodide anions.[61,144,145] Several studies have reported notable improvements in iodine adsorption due to ionic sites.

Zhang *et al.*[69] reported the synthesis of two novel nitrone-linked COFs (CityU-1 and CityU-2) through the Kröhnke oxidation reaction, by ingeniously designing precursors containing multiple nitroso groups and precisely controlling

 This journal is © The Royal Society of Chemistry 2025

Published on 02 mis Genver 2025. Downloaded on 06/02/2026 05:45:19.

polymerization conditions. CityU-1 exhibits good iodine adsorption capacity (3.0 g $g^{-1}$). Han *et al.*[66] reported using a multicomponent synthesis strategy to construct ionic COFs with high surface area, high pore volume, and a high density of iodine capture sites (as shown in Fig. 14(A)). By adjusting the ratio of aldehyde monomers, they tailored the proportions of –OH and –$OCH_3$ groups in the framework, synthesizing a series of COF-OH-*X*. These were further modified with (2-bromoethyl) trimethylammonium bromide to prepare iCOF-AB-*X*, using the –OH groups as reaction sites. Among these, iCOF-AB-50 exhibited the best performance, with a $Q_e$ of 10.2 g $g^{-1}$ and a dynamic adsorption capacity of 2.7 g $g^{-1}$. Compared to the neutral precursor COF-AB-50 ($k_{80\%}$ = 0.18 g $g^{-1}$ $h^{-1}$), the iodine adsorption kinetics of iCOF-AB-50 ($k_{80\%}$ = 1.19 g $g^{-1}$ $h^{-1}$) were significantly improved. Raman spectroscopy and XPS analyses indicated that ionic groups greatly enhance iodine adsorption by interacting with different iodine species and calculating their binding energies. Similarly, Bu, Li, and Han *et al.*[146] synthesized guanidine-based COF TGDM (as shown in Fig. 14(B)) using thiourea hydrochloride and 2,5-dimethoxyterephthaldehyde as monomers. Experimental characterization and theoretical calculations revealed multiple adsorption sites in TGDM, including C═N, –$OCH_3$, phenyl rings, and ionic sites, but only ionic sites could capture and fix iodine at high temperatures through strong Coulomb interactions. Under simulated industrial conditions of 150 °C and 150 ppmv $I_2$, TGDM achieved an iodine adsorption rate of ~30 wt%, significantly outperforming industrial silver-based adsorbents such as Ag@MOR with a 17 wt% rate.

Ghosh *et al.*[147] found that ionic frameworks have unique advantages in immobilizing polyiodide ions. They reported two ionic polymers, compound-1 and compound-2, which included benzene rings, imidazolium cations, and bromide anions as three synergistic adsorption sites, promoting the adsorption of $I_2/I_3^-$. These polymers exhibited gaseous iodine adsorption capacities of ~7.0 g $g^{-1}$ and ~4.0 g $g^{-1}$, respectively. The study demonstrated that the ionic nature of the polymers endowed them with exceptional iodine affinity, capable of capturing iodine from seawater and removing $I_3^-$ from water with a removal rate exceeding 99% within 30 minutes. Although ion-functionalized COFs show remarkable iodine adsorption capabilities, research on ionic COF adsorbents is still in its early stages and requires further exploration.

### 5.4 COF nanosheets

Utilizing ionic sites through Coulomb interactions and hydrogen/halogen bond induction, COFs can achieve both high iodine adsorption capacity and enhanced adsorption rates.

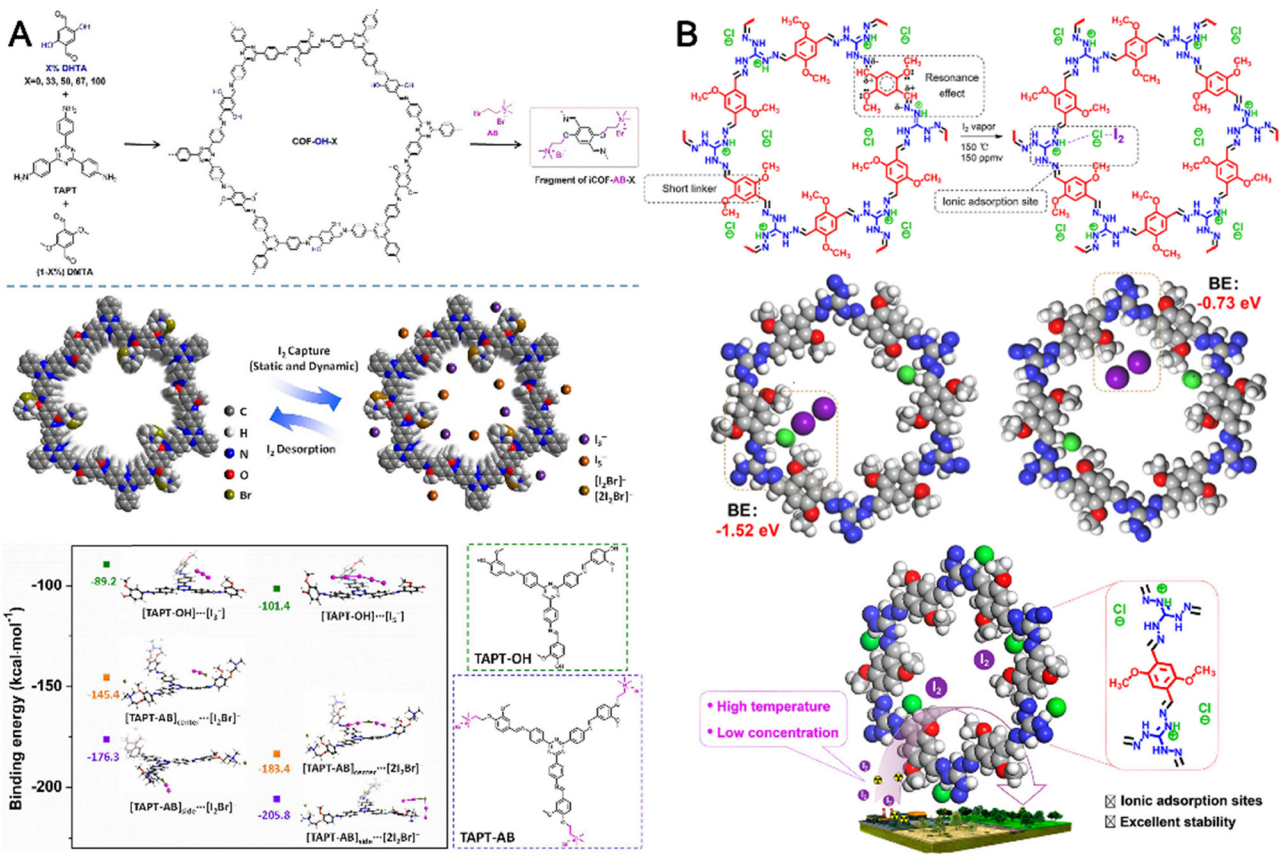


Fig. 14 Construction of ionic COFs adsorbents using quaternization strategy. (A) Study on the synthesis of ionic COFs and their adsorption mechanism after ionic liquid grafting. Reproduced with permission from ref. 66. Copyright©2021 Wiley-VCH GmbH. (B) Synthesis and interaction mechanism of ionic guanidine-based COFs adsorbents. Reproduced with permission from ref. 146. Copyright©2022 American Chemical Society.

Published on 02 mis Genver 2025. Downloaded on 06/02/2026 05:45:19.

In principle, ionic site functionalization of COFs can be achieved by designing suitable monomers or employing post-synthetic modification strategies.[145] However, practically integrating ionic sites into COF frameworks while maintaining crystallinity and inherent porosity presents significant challenges.[144] In several studies involving post-synthetic modifications of COFs, introducing chemical adsorption sites often leads to sacrifices in inherent structural characteristics, such as reduced crystallinity, surface area, pore size, and pore volume, for example resulting in COF nanosheets.[148] Despite these reductions, substantial improvements in both the $Q_e$ and $k_{80\%}$ have been observed.

Our group[68] reported a method called Ionic Liquid Solution Processing (ILSP), which can significantly increase the $k_{80\%}$ of COFs for gaseous iodine (Fig. 15(A)). In this study, an amino triazolium ionic liquid was used to modify the oxygen-containing acid COF, $TpPaSO_3H$ ($k_{80\%}$ = 0.51 g g$^{-1}$ h$^{-1}$), through the ILSP method for ion exchange modification. This process successfully prepared ionic COF nanosheets, $AC_4trimTpPaSO_3$-100, with its $k_{80\%}$ value increased fivefold to 2.1 g g$^{-1}$ h$^{-1}$. The successful introduction of ionic sites led to the transformation of $AC_4trimTpPaSO_3$-100 from bulk crystals to COF nanosheets, sacrificing crystallinity and inherent pores. A series of experimental results and theoretical analyses indicated that the significant improvement in $k_{80\%}$ was attributed to the following two factors: (1) the morphology of COF nanosheets exposed more ionic adsorption sites that could be rapidly accessed; (2) the substitution of large-volume amino triazolium cation led to the local charge separation of the COF framework, promoting non-bonding interactions between ionic sites and iodine. Additionally, our group[90] also discovered a mobile cationic hydrogen bond donor in Bmim-$TpPaSO_3$ COF nanosheets, which facilitated iodine adsorption (Fig. 15(B)). It was found that Bmim-$TpPaSO_3$ provided mobile hydrogen bond donors in its nanochannels, significantly enhancing the iodine adsorption performance ($k_{80\%}$ is 2.86 g g$^{-1}$ h$^{-1}$, $Q_e$ is 5.25 g g$^{-1}$), compared to Tp$Pa$-$SO_3H$ with fixed hydrogen bond donors ($k_{80\%}$ is 0.51 g g$^{-1}$ h$^{-1}$, $Q_e$ is 1.5 g g$^{-1}$). Both experimental and theoretical studies demonstrated that the introduction of hydrogen bond donors enhanced the interaction between Bmim-$TpPaSO_3$ and iodine, facilitating the fixation of polyiodide anions and inducing the sulfonic group of Bmim-$TpPaSO_3$ to convert iodine molecules into polyiodide ions through a charge transfer mechanism. Further investigation[149] revealed that the ability of $-SO_3^-$ to interact with $I_2$ could be controlled by changing the electrophilicity of the

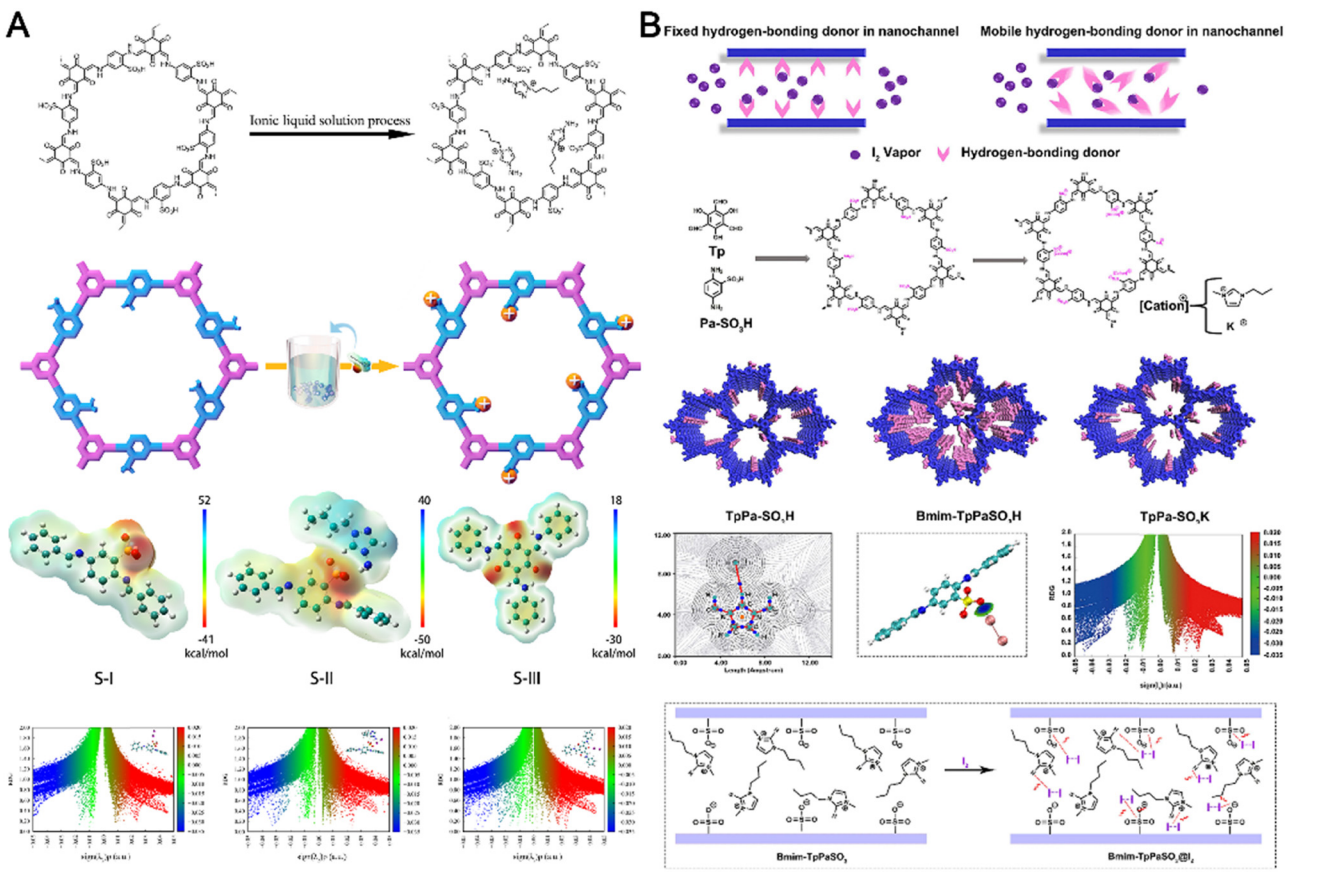


Fig. 15 Preparation of ionic COF nanosheet adsorbents by Ionic Liquid Solution Process (ILSP). (A) Preparation of ionic COF nanosheet adsorbents using ILSP strategy and analysis of their structure and adsorption mechanism. Reproduced with permission from ref. 68. Copyright©2023 Wiley-VCH GmbH. (B) ILSP construction of mobile hydrogen bonding donors in ionic COF nanosheet and analysis of their iodine adsorption enhancement mechanism. Reproduced with permission from ref. 90. Copyright©2024 Elsevier B.V.

 This journal is © The Royal Society of Chemistry 2025

Published on 02 mis Genver 2025. Downloaded on 06/02/2026 05:45:19.

cation on the ionic site "–$SO_3^-$ $[Cation]^+$" on the COF nanosheets. As the electrophilicity of the cation on the ionic structure approached $I_2$, the COF nanosheets exhibited higher iodine adsorption capacity and rate. During the process of electrophilicity regulation, we observed that changes in the cation caused alterations in the local electron distribution of ionic sites, resulting in an effective positive correlation between the local polarity changes of COF nanosheets and their actual adsorption performance.

### 5.5 3D/Quasi-3D COFs

Compared to 2D COFs, 3D COFs often possess a higher surface area, providing more active sites for iodine adsorption and resulting in higher adsorption capacities. Cao *et al.*[84] reported the synthesis of 3D COF-DL229 with an octahedral diamond structure using 1,3,5,7-tetra(4-aminophenyl)adamantane and 1,4-benzaldehyde as monomers. Structurally, the rigid adamantane nodes support the 3D framework, while the imine-linked phenyl edges introduce flexibility, giving COF-DL229 a "soft" 3D characteristic. COF-DL229 effectively adsorbs iodine by forming charge-transfer complexes with the pore walls, achieving an adsorption capacity of 4.7 g $g^{-1}$. Liu *et al.*[79] reported three 3D imine COFs (DbTd-COF, DpTd-COF, and DaTd-COFs) constructed from adamantane-based aldehyde monomers with biphenylamine, 2,5-diaminopyridine, and *p*-phenylenediamine. The 3D spatial structure and high surface area endowed these COFs with excellent iodine adsorption capacities, with $Q_e$ of 4.9 g $g^{-1}$, 3.4 g $g^{-1}$, and 4.3 g $g^{-1}$, respectively.

Subsequently, Ma *et al.*[64] reported a series of wheel-shaped COFs with quasi-3D topology, QTD-COF-*X* (*X* = 1, 2, 3, 4, V). These COFs have unique stereoscopic triangular pores and large interlayer spacings, attributed to their flexible structural unit CTP-6-CHO (hexakis(4-formylphenoxy)cyclotriphosphazene). These characteristics provide elastic pores and adaptive molecular transport. Among them, QTD-COF-V exhibited both rapid adsorption rate ($k_{80\%}$ is 2.51 g $g^{-1}$ $h^{-1}$) and high adsorption capacity ($Q_e$ is 6.2 g $g^{-1}$), with high radiation stability, suggesting significant potential for rapid radioactive iodine capture. The quasi-3D structures, with their more open spaces and multidirectional interconnected pores, facilitate effective iodine diffusion and penetration, accelerating mass transfer rates and shortening adsorption saturation time. Tong *et al.*[71] conducted a theoretical computational study on the structure and iodine adsorption performance of COFs, systematically evaluating the iodine and methyl iodide adsorption properties of 187 experimentally reported COFs under simulated conditions. The results indicated that 3D COFs exhibited better iodine adsorption performance than 2D COFs. The best iodine adsorbent was 3D-Py-COF, with the highest theoretical adsorption capacity of 16.7 g $g^{-1}$. The best methyl iodide adsorbent was COF-301, with a theoretical value of 2.8 g $g^{-1}$. Additionally, a new 3D-Py-COF-TANM was designed, with a theoretical adsorption capacity of 19.9 g $g^{-1}$. Despite the theoretical advantages of 3D COFs in rapid adsorption and high adsorption capacity, their complex monomer structures are challenging to synthesize. Furthermore, the interpenetrating pore characteristics of 3D COFs complicate structural analysis, significantly limiting their development and application in iodine adsorption.[150,151]

## 6. Conclusion and outlook

### 6.1 Conclusion

In this review, we have explored the potential of covalent organic frameworks (COFs) for the adsorption of radioactive iodine, emphasizing their structural characteristics, functionalization, and performance. COFs offer a unique combination of high surface area, tunable porosity, and chemical versatility, making them highly effective for capturing gaseous radioactive iodine. The intrinsic structural features of COFs, such as their porous nature, conjugated frameworks, and hydrogen bonding, play a crucial role in their adsorption efficiency. Functionalization of COFs further enhances their performance, with electron-rich, flexible, ionic, nanosheet, and quasi-3D COFs demonstrating superior iodine capture capabilities. These modifications enable COFs to accommodate different iodine species and improve their stability and reusability, addressing the limitations of traditional capture techniques.

In conclusion, COFs represent a promising solution for the adsorption of radioactive iodine, offering potential for significant improvements in nuclear waste management and environmental safety. Continued innovation and research in this field are crucial to fully realize the capabilities of COFs and address the pressing challenges associated with radioactive iodine.

### 6.2 Outlook

The future of covalent organic frameworks (COFs) in the adsorption of radioactive iodine looks promising, driven by ongoing advancements in material science and engineering. Several key areas warrant further exploration to fully harness the potential of COFs for this critical application.

Enhanced functionalization techniques: developing novel functionalization methods to introduce more diverse and effective functional groups can significantly enhance the adsorption capacity and selectivity of COFs for different iodine species. This includes the exploration of hybrid materials combining COFs with other nanostructures or metal–organic frameworks (MOFs) to create synergistic effects.

Scalable synthesis methods: to transition COFs from laboratory research to practical applications, scalable and cost-effective synthesis methods must be developed. Innovations in synthesis techniques, such as mechanochemical synthesis or green chemistry approaches, could lower production costs and environmental impact.

Real application testing: extensive testing of COFs under realistic environmental conditions, including varying temperatures, pressures, and radiation levels, is essential. This will provide valuable data on the stability, durability, and reusability of COFs in real-world scenarios.

Integration into existing systems: research should focus on integrating COFs into existing nuclear waste management and

Published on 02 mis Genver 2025. Downloaded on 06/02/2026 05:45:19.

environmental protection systems. This includes designing COF-based filters, coatings, or composites that can be easily incorporated into current technologies.

Interdisciplinary collaboration: collaboration across disciplines, including chemistry, materials science, environmental engineering, and nuclear science, will be crucial. Such interdisciplinary efforts can drive innovation and address complex challenges more effectively.

Regulatory and safety considerations: addressing regulatory and safety considerations is essential for the widespread adoption of COFs in radioactive iodine management. Research should include thorough assessments of the long-term safety, environmental impact, and regulatory compliance of COF-based solutions.

In summary, while significant progress has been made, the continued development and optimization of COFs for radioactive iodine adsorption require focused research and collaboration. By addressing the challenges and leveraging the unique properties of COFs, we can advance towards more efficient and sustainable solutions for managing radioactive iodine and protecting the environment.

## Data availability

This submission is a review; it does not contain experiments or data. All data used in this submission are from published references.

## Conflicts of interest

There are no conflicts to declare.

## References

1 G. He, R. Zhang and Z. Jiang, *Acc. Mater. Res.*, 2021, **2**, 630–643.
2 S. Xiong, X. Tang, C. Pan, L. Li, J. Tang and G. Yu, *ACS Appl. Mater. Interfaces*, 2019, **11**, 27335–27342.
3 I. R. E. A. (IRENA), Global Energy Transformation: A Roadmap to 2050, International Renewable Energy Agency, Abu Dhabi, 2019.
4 S. Mallapaty, *Nature*, 2020, **568**, 482–483.
5 Y. Yuan, Q. Yu, M. Cao, L. Feng, S. Feng, T. Liu, T. Feng, B. Yan, Z. Guo and N. Wang, *Nat. Sustain.*, 2021, **4**, 708–714.
6 I. R. E. A. (IRENA), Renewable Energy and Jobs – Annual Review 2020, International Renewable Energy Agency, Abu Dhabi, 2020.
7 M. Lenzen, *Energy Convers. Manage.*, 2008, **49**, 2178–2199.
8 R. Taylor, G. Mathers and A. Banford, *Prog. Nucl. Energy*, 2023, **164**, 104837.
9 A. Baker, A. Fells, M. J. Carrott, C. J. Maher and B. C. Hanson, *Chem. Soc. Rev.*, 2022, **51**, 3964–3999.
10 I. Kumari, B. V. R. Kumar and A. Khanna, *Nucl. Eng. Des.*, 2020, **358**, 110410.
11 J. A. Mattocks and J. A. Cotruvo, *Chem. Soc. Rev.*, 2020, **49**, 8315–8334.
12 B. E. Cowie, J. M. Purkis, J. Austin, J. B. Love and P. L. Arnold, *Chem. Rev.*, 2019, **119**, 10595–10637.
13 M. Alyapyshev, V. Babain and D. Kirsanov, *Energies*, 2022, **15**, 7380.
14 P. Fernández-Arias, D. Vergara and Á. Antón-Sancho, *Energies*, 2023, **16**, 6215.
15 M. M. Abu-Khader, *Prog. Nucl. Energy*, 2009, **51**, 225–235.
16 Z. Lu, W. Zhao, L. Wu, J. He, W. Dai, C. Zhou, H. Du and J. Ye, *Sens. Actuators, B*, 2021, **326**, 128957.
17 W. Xie, D. Cui, S.-R. Zhang, Y.-H. Xu and D.-L. Jiang, *Mater. Horiz.*, 2019, **6**, 1571–1595.
18 E. M. Cox and Y. Arai, in *Advances in Agronomy*, ed. D. L. Sparks, Academic Press, 2014, vol. 128, pp. 47–96.
19 D. Wang, Q. Zhou, Y. Yin, D. Lu, L. Hu, R. H. Richmond, H.-B. Moon, B. Yan and G. Jiang, *Environ. Sci. Technol.*, 2024, **58**, 3061–3064.
20 A. Tesfay Reda, M. Pan, D. Zhang and X. Xu, *J. Environ. Chem. Eng.*, 2021, **9**, 105279.
21 P. Côté Adrien, I. Benin Annabelle, W. Ockwig Nathan, M. O'Keeffe, J. Matzger Adam and M. Yaghi Omar, *Science*, 2005, **310**, 1166–1170.
22 C. J. Doonan, D. J. Tranchemontagne, T. G. Glover, J. R. Hunt and O. M. Yaghi, *Nat. Chem.*, 2010, **2**, 235–238.
23 S. Yang, W. Hu, X. Zhang, P. He, B. Pattengale, C. Liu, M. Cendejas, I. Hermans, X. Zhang, J. Zhang and J. Huang, *J. Am. Chem. Soc.*, 2018, **140**, 14614–14618.
24 P. Wang, Q. Xu, Z. Li, W. Jiang, Q. Jiang and D. Jiang, *Adv. Mater.*, 2018, **30**, 1801991.
25 Y. Xie, T. Pan, Q. Lei, C. Chen, X. Dong, Y. Yuan, W. A. Maksoud, L. Zhao, L. Cavallo, I. Pinnau and Y. Han, *Nat. Commun.*, 2022, **13**, 2878.
26 L. Zhai, S. Sun, P. Chen, Y. Zhang, Q. Sun, Q. Xu, Y. Wu, R. Nie, Z. Li and L. Mi, *Mater. Chem. Front.*, 2021, **5**, 5463–5470.
27 Y. Zhao, X. Liu, Y. Li, M. Xia, T. Xia, H. Sun, Z. Sui, X.-M. Hu and Q. Chen, *Microporous Mesoporous Mater.*, 2021, **319**, 111046.
28 S. Lin, S. Diercks Christian, Y.-B. Zhang, N. Kornienko, M. Nichols Eva, Y. Zhao, R. Paris Aubrey, D. Kim, P. Yang, M. Yaghi Omar and J. Chang Christopher, *Science*, 2015, **349**, 1208–1213.
29 H. Lyu, C. S. Diercks, C. Zhu and O. M. Yaghi, *J. Am. Chem. Soc.*, 2019, **141**, 6848–6852.
30 Y. Shi, J. Yang, F. Gao and Q. Zhang, *ACS Nano*, 2023, **17**, 1879–1905.
31 J. Sun, F. Kang, D. Yan, T. Ding, Y. Wang, X. Zhou and Q. Zhang, *Angew. Chem., Int. Ed.*, 2024, **63**, e202406511.
32 S. Xu and Q. Zhang, *Mater. Today Energy*, 2021, **20**, 100635.
33 J. Wang and S. Zhuang, *Coord. Chem. Rev.*, 2019, **400**, 213046.
34 C. Liu, Y. Jin, Z. Yu, L. Gong, H. Wang, B. Yu, W. Zhang and J. Jiang, *J. Am. Chem. Soc.*, 2022, **144**, 12390–12399.
35 M. Bhadra, S. Kandambeth, M. K. Sahoo, M. Addicoat, E. Balaraman and R. Banerjee, *J. Am. Chem. Soc.*, 2019, **141**, 6152–6156.
36 S. B. Alahakoon, S. D. Diwakara, C. M. Thompson and R. A. Smaldone, *Chem. Soc. Rev.*, 2020, **49**, 1344–1356.
37 S.-Y. Ding and W. Wang, *Chem. Soc. Rev.*, 2013, **42**, 548–568.
38 E. Rozhko, A. Bavykina, D. Osadchii, M. Makkee and J. Gascon, *J. Catal.*, 2017, **345**, 270–280.
39 T. Banerjee, F. Haase, G. Savasci, K. Gottschling, C. Ochsenfeld and B. V. Lotsch, *J. Am. Chem. Soc.*, 2017, **139**, 16228–16234.
40 H.-L. Qian, C.-X. Yang and X.-P. Yan, *Nat. Commun.*, 2016, **7**, 12104.
41 R. Kulkarni, Y. Noda, D. Kumar Barange, Y. S. Kochergin, P. Lyu, B. Balcarova, P. Nachtigall and M. J. Bojdys, *Nat. Commun.*, 2019, **10**, 3228.
42 H. B. Aiyappa, J. Thote, D. B. Shinde, R. Banerjee and S. Kurungot, *Chem. Mater.*, 2016, **28**, 4375–4379.
43 Y. Fu, X. Zhu, L. Huang, X. Zhang, F. Zhang and W. Zhu, *Appl. Catal., B*, 2018, **239**, 46–51.
44 V. S. Vyas, M. Vishwakarma, I. Moudrakovski, F. Haase, G. Savasci, C. Ochsenfeld, J. P. Spatz and B. V. Lotsch, *Adv. Mater.*, 2016, **28**, 8749–8754.
45 H.-L. Qian, Y. Wang and X.-P. Yan, *TrAC, Trends Anal. Chem.*, 2022, **147**, 116516.
46 Y. Yusran, X. Guan, H. Li, Q. Fang and S. Qiu, *Natl. Sci. Rev.*, 2020, **7**, 170–190.
47 R. Liu, K. T. Tan, Y. Gong, Y. Chen, Z. Li, S. Xie, T. He, Z. Lu, H. Yang and D. Jiang, *Chem. Soc. Rev.*, 2021, **50**, 120–242.
48 Z. Li, L. Sheng, H. Wang, X. Wang, M. Li, Y. Xu, H. Cui, H. Zhang, H. Liang, H. Xu and X. He, *J. Am. Chem. Soc.*, 2021, **143**, 92–96.
49 C. Kang, Z. Zhang, V. Wee, A. K. Usadi, D. C. Calabro, L. S. Baugh, S. Wang, Y. Wang and D. Zhao, *J. Am. Chem. Soc.*, 2020, **142**, 12995–13002.
50 H. Ding, A. Mal and C. Wang, *Mater. Chem. Front.*, 2020, **4**, 113–127.
51 Q. Yang, M. Luo, K. Liu, H. Cao and H. Yan, *Appl. Catal., B*, 2020, **276**, 119174.
52 C. R. DeBlase, K. E. Silberstein, T.-T. Truong, H. D. Abruña and W. R. Dichtel, *J. Am. Chem. Soc.*, 2013, **135**, 16821–16824.

 This journal is © The Royal Society of Chemistry 2025

Published on 02 mis Genver 2025. Downloaded on 06/02/2026 05:45:19.

53 Y. Liu, Y. Zhu, S. B. Alahakoon and E. Egap, *ACS Mater. Lett.*, 2020, **2**, 1561–1566.
54 G.-H. Zhang, L. Zhang, Q.-H. Zhu, H. Chen, W.-L. Yuan, J. Fu, S.-L. Wang, L. He and G.-H. Tao, *ACS Mater. Lett.*, 2021, **4**, 136–144.
55 G.-H. Zhang, Q.-H. Zhu, S.-J. Guo, L. Zhang, C. Yu, S. Qin, L. He and G.-H. Tao, *Adv. Mater.*, 2024, **36**, 2311990.
56 D. Tong, Y. Zhao, Y. Wang, Z. Han, W. Jie, J. Zhang and C. Yu, *Chem. Res. Chin. Univ.*, 2024, **45**, 20230401.
57 T. Pan, K. Yang, X. Dong and Y. Han, *J. Mater. Chem. A*, 2023, **11**, 5460–5475.
58 Y. Li, W. Chen, G. Xing, D. Jiang and L. Chen, *Chem. Soc. Rev.*, 2020, **49**, 2852–2868.
59 L. Zhang, J. Li, H. Zhang, Y. Liu, Y. Cui, F. Jin, K. Wang, G. Liu, Y. Zhao and Y. Zeng, *Chem. Commun.*, 2021, **57**, 5558–5561.
60 Y. Yang, C. Tu, H. Yin, J. Liu, F. Cheng and F. Luo, *Molecules*, 2022, **27**, 9045.
61 J. F. Kurisingal, H. Yun and C. S. Hong, *J. Hazard. Mater.*, 2023, **458**, 131835.
62 Z.-J. Yin, S.-Q. Xu, T.-G. Zhan, Q.-Y. Qi, Z.-Q. Wu and X. Zhao, *Chem. Commun.*, 2017, **53**, 7266–7269.
63 L. He, L. Chen, X. Dong, S. Zhang, M. Zhang, X. Dai, X. Liu, P. Lin, K. Li, C. Chen, T. Pan, F. Ma, J. Chen, M. Yuan, Y. Zhang, L. Chen, R. Zhou, Y. Han, Z. Chai and S. Wang, *Chem*, 2021, **7**, 699–714.
64 X. Guo, Y. Li, M. Zhang, K. Cao, Y. Tian, Y. Qi, S. Li, K. Li, X. Yu and L. Ma, *Angew. Chem., Int. Ed.*, 2020, **59**, 2697–22705.
65 M. Zhang, Y. Li, W. Yuan, X. Guo, C. Bai, Y. Zou, H. Long, Y. Qi, S. Li, G. Tao, C. Xia and L. Ma, *Angew. Chem., Int. Ed.*, 2021, **60**, 12396–12405.
66 Y. Xie, T. Pan, Q. Lei, C. Chen, X. Dong, Y. Yuan, J. Shen, Y. Cai, C. Zhou, I. Pinnau and Y. Han, *Angew. Chem., Int. Ed.*, 2021, **60**, 22432–22440.
67 Y. Huang, Z. Yu, Q. Zhang and F. Luo, *Sci. China Mater.*, 2023, **66**, 2339–2345.
68 J. Fu, J.-Y. Liu, G.-H. Zhang, Q.-H. Zhu, S.-L. Wang, S. Qin, L. He and G.-H. Tao, *Small*, 2023, **19**, 2302570.
69 F. Kang, X. Wang, C. Chen, C.-S. Lee, Y. Han and Q. Zhang, *J. Am. Chem. Soc.*, 2023, **145**, 15465–15472.
70 S.-Y. Zhang, X.-H. Tang, Y.-L. Yan, S.-Q. Li, S. Zheng, J. Fan, X. Li, W.-G. Zhang and S. Cai, *ACS Macro Lett.*, 2021, **10**, 1590–1596.
71 Y. Lan, M. Tong, Q. Yang and C. Zhong, *CrystEngComm*, 2017, **19**, 4920–4926.
72 S. An, X. Zhu, Y. He, L. Yang, H. Wang, S. Jin, J. Hu and H. Liu, *Ind. Eng. Chem. Res.*, 2019, **58**, 10495–10502.
73 Y. Li, X. Li, J. Li, W. Liu, G. Cheng and H. Ke, *Microporous Mesoporous Mater.*, 2021, **325**, 111351.
74 X. Pan, X. Qin, Q. Zhang, Y. Ge, H. Ke and G. Cheng, *Microporous Mesoporous Mater.*, 2020, **296**, 109990.
75 Y. Sun, S. Song, D. Xiao, L. Gan and Y. Wang, *ACS Omega*, 2020, **5**, 24262–24271.
76 N. Mokhtari and M. Dinari, *Sep. Purif. Technol.*, 2022, **301**, 121948.
77 Y. Li, W. Chen, W. Hao, Y. Li and L. Chen, *ACS Appl. Nano Mater.*, 2018, **1**, 4756–4761.
78 Y. Yang, X. Xiong, Y. Fan, Z. Lai, Z. Xu and F. Luo, *J. Solid State Chem.*, 2019, **279**, 120979.
79 Z. Wu, W. Wei, J. Ma, J. Luo, Y. Zhou, Z. Zhou and S. Liu, *ChemistrySelect*, 2021, **6**, 10141–10148.
80 X. Guo, Y. Tian, M. Zhang, Y. Li, R. Wen, X. Li, X. Li, Y. Xue, L. Ma, C. Xia and S. Li, *Chem. Mater.*, 2018, **30**, 2299–2308.
81 M. Zhou, Z. Li, A. Munyentwali, C. Li, H. Shui and H. Li, *Chem. – Asian J.*, 2022, **17**, e202200358.
82 B. Jiang, Y. Qi, X. Li, X. Guo, Z. Jia, J. Zhang, Y. Li and L. Ma, *Chin. Chem. Lett.*, 2022, **33**, 3556–3560.
83 G. Wang, K. Xie, F. Zhu, J. Kan, S. Li, Y. Geng and Y. Dong, *Chem. Res. Chin. Univ.*, 2022, **38**, 409–414.
84 C. Wang, Y. Wang, R. Ge, X. Song, X. Xing, Q. Jiang, H. Lu, C. Hao, X. Guo, Y. Gao and D. Jiang, *Chem. – Eur. J.*, 2018, **24**, 585–589.
85 J. Li, H. Zhang, L. Zhang, K. Wang, Z. Wang, G. Liu, Y. Zhao and Y. Zeng, *J. Mater. Chem. A*, 2020, **8**, 9523–9527.
86 S. Song, Y. Shi, N. Liu and F. Liu, *ACS Appl. Mater. Interfaces*, 2021, **13**, 10513–10523.
87 R. Chen, T. Hu, W. Zhang, C. He and Y. Li, *Microporous Mesoporous Mater.*, 2021, **312**, 110739.
88 X. Yan, Y. Yang, G. Li, J. Zhang, Y. He, R. Wang, Z. Lin and Z. Cai, *Chin. Chem. Lett.*, 2023, **34**, 107201.
89 J. Chang, H. Li, J. Zhao, X. Guan, C. Li, G. Yu, V. Valtchev, Y. Yan, S. Qiu and Q. Fang, *Chem. Sci.*, 2021, **12**, 8452–8457.
90 J.-Y. Liu, L. Zhang, J. Fu, S.-L. Wang, Y.-R. Zhou, Y.-H. Wang, S. Qin, G.-H. Tao and L. He, *Sep. Purif. Technol.*, 2024, **331**, 125664.
91 S. I. Stepanov and A. V. Boyarintsev, *Nucl. Eng. Technol.*, 2022, **54**, 2339–2358.
92 Y. Yang, C. Tu, L. Guo, L. Wang, F. Cheng and F. Luo, *Cell Rep. Phys. Sci.*, 2023, **4**, 101694.
93 Y.-Q. Xiang, Y.-H. Wang, H. Chen, J. Fu, Q.-H. Zhu, X.-L. Yang, X.-H. Xu, S. Qin, L. He and G.-H. Tao, *Chem. Eng. J.*, 2023, **456**, 140979.
94 N. R. Soelberg, T. G. Garn, M. R. Greenhalgh, J. D. Law, R. Jubin, D. M. Strachan and P. K. Thallapally, *Sci. Technol. Nucl. Install.*, 2013, **2013**, 702496.
95 Y. Onda, K. Taniguchi, K. Yoshimura, H. Kato, J. Takahashi, Y. Wakiyama, F. Coppin and H. Smith, *Nat. Rev. Earth Environ.*, 2020, **1**, 644–660.
96 X. Hou, V. Hansen, A. Aldahan, G. Possnert, O. C. Lind and G. Lujaniene, *Anal. Chim. Acta*, 2009, **632**, 181–196.
97 S.-J. Guo, G.-H. Zhang, Q.-H. Zhu, C. Yu, J.-Y. Liu, X.-L. Yang, S. Qin, N.-R. Zhao, L. He and G.-H. Tao, *Chem. Eng. J.*, 2023, **475**, 146221.
98 G. G. Eichholz, *Nucl. Technol.*, 1983, **69**, 120.
99 R. T. Jubin, D. M. Strachan and N. R. Soelberg, Iodine Pathways and Off-Gas Stream Characteristics for Aqueous Reprocessing Plants – A Literature Survey and Assessment, Report Report No. INL/EXT-13-30119, Idaho National Lab. (INL), United States, 2013.
100 T. Sakuragi, R. Hamada, M. Harigai, H. Asano, T. Oniki and R. Ito, *MRS Adv.*, 2024, **9**, 415–419.
101 G. Sgouros, L. Bodei, M. R. McDevitt and J. R. Nedrow, *Nat. Rev. Drug Discovery*, 2020, **19**, 589–608.
102 D. Gombert, W. Ebert, J. Marra, R. Jubin and J. Vienna, Global Nuclear Energy Partnership Waste Treatment Baseline, Report Report No. INL/CON-08-13917, Idaho National Lab. (INL), United States, 2008.
103 J. Huve, A. Ryzhikov, H. Nouali, V. Lalia, G. Augé and T. J. Daou, *RSC Adv.*, 2018, **8**, 29248–29273.
104 S. U. Nandanwar, K. Coldsnow, V. Utgikar, P. Sabharwall and D. Eric Aston, *Chem. Eng. J.*, 2016, **306**, 369–381.
105 B. Li, X. Dong, H. Wang, D. Ma, K. Tan, S. Jensen, B. J. Deibert, J. Butler, J. Cure, Z. Shi, T. Thonhauser, Y. J. Chabal, Y. Han and J. Li, *Nat. Commun.*, 2017, **8**, 485.
106 K. Umadevi and D. Mandal, *J. Environ. Radioact.*, 2021, **234**, 106623.
107 T. Shimura, I. Yamaguchi and N. Kunugita, in *Encyclopedia of Environmental Health*, ed. J. Nriagu, Elsevier, Oxford, 2nd edn, 2019, vol. 10974-1, pp. 96–106.
108 S. Jablon, Z. Hrubec and J. D. Boice, *IAEA Bull.*, 1991, **33**, 2.
109 C. Aceves, I. Mendieta, B. Anguiano and E. Delgado-González, *Int. J. Mol. Sci.*, 2021, **22**, 1228.
110 R. T. Jubin, N. Soelberg and D. M. Strachan, Position Paper on Practicable Performance Criteria for the Removal Efficiency of Volatile Radionuclides, Report Report No. INL/EXT-12-25410, Idaho National Lab. (INL), United States, 2012.
111 S. H. Bruffey, L. R. Martin, K. M. Peruski and N. R. Soelberg, Fuel age impacts on gaseous fission product capture during separations, Report Report No. PNNL-22550, Pacific Northwest National Lab. (PNNL), United States, 2012.
112 H. Mineo, M. Iizuka, S. Fujisaki, S. Hotoku, T. Asakura and G. Uchiyama, Study on Gaseous Effluent Treatment for Dissolution Step of Spent Nuclear Fuel Reprocessing, Waste Management 2002 Symposium, United States, 2002.
113 W. A. Reed, I. May, F. R. Livens, J. M. Charnock, A. P. Jeapes, M. Gresley, R. M. Mitchell and P. Knight, *J. Anal. At. Spectrom.*, 2002, **17**, 541–543.
114 T. Sakurai and A. Takahashi, Behavior of iodine in the reprocessing of spent nuclear fuels. Research and survey, Report Report No. JAERI-Review-97-002, Japan Atomic Energy Research Inst., Japan, 1997.
115 L. L. Burger and R. D. Scheele, Status of radioiodine control for nuclear fuel reprocessing plants, Report Report No. PNL-4689, Pacific Northwest National Lab. (PNNL), United States, 1983.
116 B. J. Riley, J. D. Vienna, D. M. Strachan, J. S. McCloy and J. L. Jerden, *J. Nucl. Mater.*, 2016, **470**, 307–326.
117 C. Muhire, A. Tesfay Reda, D. Zhang, X. Xu and C. Cui, *Chem. Eng. J.*, 2022, **431**, 133816.
118 C. Zhao, L. Ge, M. Zuo, L. Mai, S. Chen, X. Li, Q. Li, Y. Wang and C. Xu, *Energy*, 2023, **282**, 128450.

Published on 02 mis Genver 2025. Downloaded on 06/02/2026 05:45:19.

119 T. C. T. Pham, S. Docao, I. C. Hwang, M. K. Song, D. Y. Choi, D. Moon, P. Oleynikov and K. B. Yoon, *Energy Environ. Sci.*, 2016, **9**, 1050–1062.
120 A. Tesfay Reda, D. Zhang, X. Xu and S. Xu, *Sep. Purif. Technol.*, 2022, **292**, 120994.
121 C. Bläker, J. Muthmann, C. Pasel and D. Bathen, *ChemBioEng Rev.*, 2019, **6**, 119–138.
122 R. Ganjoo, S. Sharma, A. Kumar and M. M. A. Daouda, in *Activated Carbon: Progress and Applications*, ed. C. Verma and M. A. Quraishi, The Royal Society of Chemistry, 2023.
123 R. C. Moore, C. I. Pearce, J. W. Morad, S. Chatterjee, T. G. Levitskaia, R. M. Asmussen, A. R. Lawter, J. J. Neeway, N. P. Qafoku, M. J. Rigali, S. A. Saslow, J. E. Szecsody, P. K. Thallapally, G. Wang and V. L. Freedman, *Sci. Total Environ.*, 2020, **716**, 132820.
124 K. W. Chapman, P. J. Chupas and T. M. Nenoff, *J. Am. Chem. Soc.*, 2010, **132**, 8897–8899.
125 Y. Li and J. Yu, *Nat. Rev. Mater.*, 2021, **6**, 1156–1174.
126 J. Zhou, T. Lan, T. Li, Q. Chen, P. Bai, F. Liu, Z. Yuan, W. Zheng, X. Luo, W. Yan and T. Yan, *Sep. Purif. Technol.*, 2022, **290**, 120895.
127 M. S. Chavali and M. P. Nikolova, *SN Appl. Sci.*, 2019, **1**, 607.
128 Z. Jia, Z. Yan, J. Zhang, Y. Zou, Y. Qi, X. Li, Y. Li, X. Guo, C. Yang and L. Ma, *ACS Appl. Mater. Interfaces*, 2021, **13**, 1127–1134.
129 S. Yang, X. Li, Y. Qin, Y. Cheng, W. Fan, X. Lang, L. Zheng and Q. Cao, *ACS Appl. Mater. Interfaces*, 2021, **13**, 29471–29481.
130 X. Wu, X. Han, Y. Liu, Y. Liu and Y. Cui, *J. Am. Chem. Soc.*, 2018, **140**, 16124–16133.
131 Q. Jiang, H. Huang, Y. Tang, Y. Zhang and C. Zhong, *Ind. Eng. Chem. Res.*, 2018, **57**, 15114–15121.
132 L. Zhang, Y.-T. Luo, J.-Q. Fan, S.-J. Xiao, Q.-Q. Zheng, X.-L. Liu, Q.-G. Tan, C. Sun, Q. Shi, R.-P. Liang and J.-D. Qiu, *J. Hazard. Mater.*, 2024, **465**, 133488.
133 Q. Wu, Q.-Q. Jiang, Y.-J. Li, Y.-A. Wang, X. Wang, R.-P. Liang and J.-D. Qiu, *Anal. Chem.*, 2024, **96**, 4623–4631.
134 Y. Lin, X. Jiang, S. T. Kim, S. B. Alahakoon, X. Hou, Z. Zhang, C. M. Thompson, R. A. Smaldone and C. Ke, *J. Am. Chem. Soc.*, 2017, **139**, 7172–7175.
135 B. Li, W. Qiu, G. P. A. Yap, Y. L. Dory and J. P. Claverie, *Adv. Funct. Mater.*, 2023, **34**, 2311964.
136 A. Samui, Happy and S. K. Sahu, *Microporous Mesoporous Mater.*, 2020, **291**, 109700.
137 E. A. Gendy, D. T. Oyekunle, J. Ifthikar, A. Jawad and Z. Chen, *Environ. Sci. Pollut. Res.*, 2022, **29**, 32566–32593.
138 K. Geng, T. He, R. Liu, S. Dalapati, K. T. Tan, Z. Li, S. Tao, Y. Gong, Q. Jiang and D. Jiang, *Chem. Rev.*, 2020, **120**, 8814–8933.
139 X. Li, Q. Su, K. Luo, H. Li, G. Li and Q. Wu, *Mater. Lett.*, 2021, **282**, 128704.
140 W. Ji, P. Zhang, G. Feng, Y.-Z. Cheng, T.-X. Wang, D. Yuan, R. Cha, X. Ding, S. Lei and B.-H. Han, *Nat. Commun.*, 2023, **14**, 6049.
141 J. Li, J. Jia, J. Suo, C. Li, Z. Wang, H. Li, V. Valtchev, S. Qiu, X. Liu and Q. Fang, *J. Mater. Chem. A*, 2023, **11**, 18349–18355.
142 C. Ji, C. Kang, C. Patra Bidhan and D. Zhao, *CCS Chem.*, 2023, **6**, 856–881.
143 Y. Ge, J. Li, Y. Meng and D. Xiao, *Nano Energy*, 2023, **109**, 108297.
144 X. Liang, Y. Tian, Y. Yuan and Y. Kim, *Adv. Mater.*, 2021, **33**, 2105647.
145 P. Zhang, Z. Wang, P. Cheng, Y. Chen and Z. Zhang, *Coord. Chem. Rev.*, 2021, **438**, 213873.
146 Z. Zhang, X. Dong, J. Yin, Z.-G. Li, X. Li, D. Zhang, T. Pan, Q. Lei, X. Liu, Y. Xie, F. Shui, J. Li, M. Yi, J. Yuan, Z. You, L. Zhang, J. Chang, H. Zhang, W. Li, Q. Fang, B. Li, X.-H. Bu and Y. Han, *J. Am. Chem. Soc.*, 2022, **144**, 6821–6829.
147 A. Sen, S. Sharma, S. Dutta, M. M. Shirolkar, G. K. Dam, S. Let and S. K. Ghosh, *ACS Appl. Mater. Interfaces*, 2021, **13**, 34188–34196.
148 L. Chen, M. Huang, B. Chen, C. Gong, N. Li, H. Cheng, Y. Chen, Y. Peng and G. Xu, *Chin. Chem. Lett.*, 2022, **33**, 2867–2882.
149 J. Fu, J.-Y. Liu, Y.-R. Zhou, L. Zhang, S.-L. Wang, S. Qin, M. Fan, G.-H. Tao and L. He, *Chem. Eng. J.*, 2024, **488**, 150913.
150 Q. Fang, J. Wang, S. Gu, R. B. Kaspar, Z. Zhuang, J. Zheng, H. Guo, S. Qiu and Y. Yan, *J. Am. Chem. Soc.*, 2015, **137**, 8352–8355.
151 G. Lin, H. Ding, D. Yuan, B. Wang and C. Wang, *J. Am. Chem. Soc.*, 2016, **138**(10), 3302–3305.

 This journal is © The Royal Society of Chemistry 2025